A Four-Dimensional Ensemble-Variational (4DEnVar) Data Assimilation System for Global NWPs: System Description and Primary Tests

S. J. Zhu[1], B. Wang[2,1,4,5], L. Zhang[3], J. J. Liu[2,4], Y. Z. Liu[3], J. D. Gong[3], S. M. Xu[1], Y. Wang[1], W. Y. Huang[1], L. Liu[1], Y. J. He[2] and X. J. Wu[3]

[1]Department of Earth System Science, Tsinghua University, Beijing 100084, China.

[2]State Key Laboratory of Numerical Modelling for Atmospheric Sciences and Geophysical Fluid Dynamics, Institute of Atmospheric Physics, Chinese Academy of Sciences, Beijing, 100029, China.

[3]Research and Development Division, Numerical Weather Prediction Center of China Meteorological Administration, Beijing, 100081, China

[4]Innovation Group 311020008, Southern Marine Science and Engineering Guangdong Laboratory, Zhuhai, China

[5]School of Ocean, University of Chinese Academy of Sciences, Qingdao, 266400, China.

Corresponding author: Bin Wang (wab@lasg.iap.ac.cn)

Key Points:

- A DRP-4DVar-based 4DEnVar data assimilation system with the flow-dependent BEC was developed for global numerical weather predictions

- The deterministic forecast initialized from the 4DEnVar ensemble mean analysis has comparable performance to the 4DVar system

- Higher quality of analyses and ensemble forecasts can be produced by the 4DEnVar system relative to the 4DVar system

Abstract

A four-dimensional ensemble-variational (4DEnVar) data assimilation (DA) system was developed for global numerical weather predictions (NWPs). Instead of using the adjoint technique, this system utilizes a dimension-reduced projection (DRP) technique to minimize the cost function of the standard four-dimensional variational (4DVar) DA. It dynamically predicts ensemble background error covariance (BEC) initialized from its previous inflated analyses and realizes the flow-dependence of BEC in the variational configuration during the assimilation cycle. These inflated analyses, linear combinations of the ensemble analyses increment and balanced random perturbations, aim to prevent the predicted BEC from underestimation as well as to implicitly achieve the hybrid of the flow-dependent and static BEC matrices. A limited number of leading eigenvectors of the localization correlation function are selected to filter out the spurious correlations in the BEC matrix (B-matrix). In order to evaluate the new system, single-point observation experiments (SOEs) and observing system simulation experiments (OSSEs) were conducted with sounding and cloud-derived wind data. The flow-dependent characteristic was verified in the SOEs that utilized the localized ensemble covariance and compared with that of 4DVar. In the OSSEs, 4DEnVar reduced the analysis errors compared with 4DVar. The deterministic forecast initialized from the 4DEnVar ensemble mean analysis has better (worse) performance in the medium-range (long-range) forecasts in the Northern Extratropics and opposite performance in the Southern Extratropics, and exhibits slightly worse effects in the Tropics. Moreover, the ensemble mean forecast initialized from the 4DEnVar ensemble analyses has higher forecast skills than 4DVar.

Plain Language Summary

Medium-range numerical weather prediction (NWP) is of great significance to disaster mitigation and improvement of human living standards. It aims to predict weather states for future 1-10 days from the current state by solving the initial value problem of a set of partial differential equations. Data assimilation (DA) is one of the key techniques to improve forecast skills, which attempts to provide an optimal estimation of the current state by combining observations and forecasts. This study developed a four-dimensional ensemble-variational (4DEnVar) DA system for global NWPs using the dimension-reduced projection (DRP) four-dimensional variational

51   (4DVar) approach. Compared with the standard 4DVar, which is generally recognized as one of

52   the most advanced DA methods, this new system has three unique features. First, it dynamically

53   estimates background error covariance (BEC) in the DA cycle instead of adopting a pre-estimated

54   static BEC as 4DVar does. Second, it uses an ensemble covariance without the Gaussian error

55   assumption as in 4DVar. Third, it can avoid using adjoint models and handle nonlinear problems

56   well. It shows more obvious flow-dependence of the BEC, smaller analysis errors, and better

57   ensemble mean forecast skills than 4DVar, and comparable skills of deterministic forecast

58   initialized from the ensemble mean analysis to 4DVar.

1 Introduction

Accurately predicting future weather and climate states is of great significance to disaster mitigation and to the improvement of human living standards. The accuracy of global numerical weather prediction (NWP) can be significantly improved through the use of new types of data such as from satellites (Simmons & Hollingsworth, 2002). Therefore, it is necessary to develop an effective data assimilation (DA) system to make good use of observations to provide more accurate initial conditions (ICs) for NWPs.

The four-dimensional variational (4DVar) DA is recognized as one of the most advanced DA methods. This method produces the analysis field constrained dynamically and physically (Rabier et al., 2000; Wang et al., 2010a), and implicitly implements the flow-dependent background error covariance (BEC) matrix (B-matrix), which propagates information within the assimilation window by the tangent linear model (TLM) and the adjoint model (ADM; Lorenc, 2003). The uses of the ADM (Lewis & Derber, 1985; Le Dimet & Talagrand, 1986) and the incremental 4DVar scheme (Courtier et al. 1994) make the operational application of 4DVar possible (Rabier et al., 2000; Gauthier & Thépaut, 2001; Koizumi et al., 2005; Rawlins et al., 2007; Gauthier et al., 2007; Zhang et al., 2019). However, this advanced DA method has not been applied in most NWP centers in the world, except for very few major advanced centers, e.g., the European Centre for Medium-range Weather Forecasts (ECMWF). In addition, the standard 4DVar approach fails to dynamically update the B-matrix during the assimilation cycle, given that it uses the modeled climatological covariance model that can only be implicitly developed within the assimilation window (Buehner et al., 2010a).

Ensemble Kalman Filter (EnKF) is another commonly used ensemble DA method. It is based on the Monte Carlo method that uses a number of ensembles to estimate the B-matrix with the explicit flow-dependent characteristic spanning the assimilation windows (Evensen, 1994) without modeling the B-matrix nor using the ADM. Moreover, EnKF has the advantage of saving time, implicitly through concurrently generating the ensembles on a parallel computer system due to the mutual independence of ensemble members. Due to these advantages, EnKF has been applied to many models, e.g., the National Centers for Environmental Prediction (NCEP) Global Forecast System (GFS) Model (Whitaker et al., 2008, 2009), the Global Environmental Multiscale (GEM) Model (Buehner et al., 2010a, 2010b). There have been some studies comparing the

89   performance of the variational and EnKF systems. Whitaker et al. (2008) compared 3DVar and

90   EnKF using low-resolution operational model and observations, except satellite radiation, and

91   found that the ensemble system outperforms the 3DVar system, especially in data-sparse areas.

92   Whitaker et al. (2009) further compared 3DVar, 4DVar and EnKF using sparse surface pressure

93   observations, and discovered that 4DVar and EnKF have comparable performance. Buehner et al.

94   (2010b) found slight degradations (improvements) in the short-range (medium-range) forecasts

95   based on the EnKF ensemble mean analysis over the 4DVar-based forecasts in the Extratropics.

96   There is not enough evidence to prove that the forecast provided by EnKF is better than that

97   provided by 4DVar for the NWP models. Also, it is noted that the limited size of ensembles can

98   result in sampling errors in the ensemble B-matrix.

99   However, the ensemble method can provide the explicit flow-dependent information for

100   the variational method (Houtekamer et al., 2005; Whitaker et al., 2008, 2009; Buehner et al.,

101   2010a, 2010b). Likewise, the variational method can supply the ensemble method with proven

102   modules, e.g., quality control and minimization iteration modules (Courtier et al. 1994; Zhang et

103   al., 2019). Therefore, several hybrid DA methods combining the variational and ensemble ideas

104   have continuously been developed (Hamill & Snyder, 2000; Lorenc, 2003; Qiu et al., 2007; Liu et

105   al., 2008, 2009; Tian et al., 2008, 2011; Wang et al., 2010a).

106   Different methods of incorporating the ensemble covariance make the classification of

107   hybrid methods different. The hybrid ensemble-4DVar methods are mainly divided into En4DVar

108   methods that include the ADM and 4DEnVar methods that avoid the ADM. En4DVar methods

109   typically incorporate the ensemble covariance into the variational framework by a weighted sum

110   of the static and ensemble covariances (Hamill & Snyder, 2000) or extending the original control

111   variables by the control variables preconditioned by the square root of the ensemble covariance

112   (Lorenc, 2003). Also, En4DVar methods can use the ensemble information to estimate the

113   parameters of the covariance model for variational systems (Lei et al., 2020). In addition, the

114   effects of the hybrid BEC on forecast skills have been investigated in simple models (Hamill &

115   Snyder, 2000), regional models (Wang et al., 2008a, 2008b; Zhang & Zhang, 2012) and global

116   models (Raynaud et al., 2011; Bonavita et al., 2012; Buehner et al., 2010a, 2010b, 2013, 2015;

117   Clayton et al., 2013; Lorenc, 2015; Wang et al., 2013; Wang & Lei, 2014; Kleist & Ide, 2015a,

118   2015b).

119　4DEnVar method, which applies the variational framework and the idea of using ensembles
120　valid at multiple time slots to avoid the ADM to obtain the optimal analysis, is an efficient DA
121　method. Several ensemble-based methods, which can reduce the dimension from the model space
122　to a subspace composed of a limited number of base vectors in optimization and avoid the use of
123　the ADM, have been proposed in recent decade (Qiu et al., 2007; Tian et al., 2008; Wang et al.,
124　2010a). The dimension-reduced projection 4DVar (DRP-4DVar) is one of the 4DEnVar methods
125　that has been successfully applied in regional meso-scale weather forecasts (Wang et al., 2010a;
126　Zhao & Wang, 2010; Liu & Wang, 2011; Zhao et al., 2012) and global decadal climate predictions
127　(He et al., 2017, 2020a, 2020b; Li et al., 2021a, 2021b; Shi et al., 2021). In global medium-range
128　NWPs, this approach has not been widely applied and systematically evaluated, although a DRP-
129　4DVar system (Shen et al., 2015) was preliminarily established using an old version of the global
130　forecast system of the Global/Regional Assimilation and Prediction System (GRAPES-GFS)
131　based on the 3DVar system of this version (Chen et al., 2008; Xue et al., 2008). This method uses
132　a limited number of base vectors composed of initial perturbations to project the incremental
133　analysis in model space onto a low-dimensional subspace spanned by these base vectors, and
134　directly obtains an optimal analysis solution to the minimization of the 4DVar cost function in the
135　subspace. Furthermore, this method calculates the gradient of the cost function based on the
136　statistical relationship between the model space and observation space, thereby avoiding the use
137　of the ADM (Wang et al., 2010a).

138　The limited ensemble size may result in introducing sampling errors, which can lead to
139　spurious correlations in the B-matrix (Evensen, 2003), and localization techniques (Liu et al.,
140　2009; Hamill et al., 2001; Wang et al., 2010b, 2018) can effectively alleviate the aforementioned
141　problem and ameliorate analyses and forecasts. Given that conducting localization in model space
142　is quite inconvenient in implementation and computationally expensive for the non-sequential
143　ensemble methods, adopting ensemble-sample-based subspace localization schemes is thought to
144　be an economical choice (Wang et al, 2018). Localization is typically conducted as a Schür product
145　between the ensemble-based B-matrix and the correlation matrix composed of the elements
146　calculated by the correlation model related with their coordinates, so how to decompose the
147　correlation matrix to avoid the expensive multiplication between high-dimensional matrices
148　caused by the Schür product is the key to reduce computational costs. A limited number of leading
149　eigenvectors expressed by orthogonal functions (e.g., empirical orthogonal function, sine function

150 and spherical harmonic function) were used to expand the correlation function so that the high-
151 dimensional correlation matrix is decomposed into the sum of a set of products between an
152 eigenvector and its transpose (Liu et al., 2009; Buehner et al., 2010a, 2010b; Bishop et al., 2011;
153 Kuhl et al., 2013; Wang et al., 2010b, 2018). This approach not only alleviates the spurious
154 correlations and rank deficiency of the B-matrix, but also efficiently produces the extended
155 ensemble samples, which converts a very costly Schür product between two high-dimension
156 matrices to much more economical Schür products between ensemble samples and eigenvectors.

157   Motivated by these studies, many research and operational centers have not only
158 established their standalone variational systems, but also have been developing hybrid DA systems
159 for their global NWPs. These centers realized the explicit flow-dependence of the B-matrix based
160 on the original standard 4DVar framework, so that the forecast skills were further improved. The
161 ECMWF (Bonavita et al., 2012) and Météo-France (Raynaud et al., 2011) have developed hybrid
162 DA systems, which include ensemble information estimated by an ensemble of 4DVars. The Met
163 Office incorporated the flow-dependent BEC estimated by EnKF into the 4DVar system to develop
164 a hybrid system (Clayton et al., 2013). Unlike these systems relying on the ADM, some centers
165 have developed 4DEnVar systems avoiding the use of the ADM. Environment Canada combined
166 the static BEC with the 4D ensemble BEC obtained from EnKF to develop a 4DEnVar system,
167 which is considered to be a potential alternative to 4DVar considering the simplicity,
168 computational efficiency and forecast quality (Buehner et al., 2010a, 2010b, 2013, 2015). The Met
169 Office developed a hybrid 4DEnVar system (Lorenc et al., 2015; Bowler et al., 2017a) and used
170 an ensemble of 4DEnVars instead of the ETKF system to generate ensembles for the hybrid system
171 (Bowler et al., 2017b). Wang et al. (2013) and Kleist & Ide (2015a) proved the benefits of
172 including ensemble BECs into 3DVar. Then, perturbations valid at multiple time slots during the
173 assimilation window were used to estimate the 4D ensemble BEC to develop a 4DEnVar system
174 in NCEP (Wang et al., 2014; Kleist & Ide., 2015b).

175   This study focuses on developing a 4DEnVar system for global NWPs based on the DRP-
176 4DVar approach, which not only can be an alternative to DA system to provide deterministic
177 forecasts, but also to provide ensemble forecasts for hybrid systems. Compared with the theoretical
178 DRP-4DVar proposed by Wang et al (2010a), the method used for the 4DEnVar system was
179 improved in its inflation, localization and sampling. The successful applications of the 4DEnVar
180 algorithm and economical localization technique provide a good foundation to develop the

181   4DEnVar system. As the first and necessary step to evaluate the impact of the 4DEnVar system

182   on analyses and forecasts, single-point observation experiments (SOEs) and observing system

183   simulation experiments (OSSEs) were conducted. SOEs are easy to study the flow-dependent

184   characteristic of the BEC. OSSEs can help us evaluate the realistic analysis error because the

185   "truth" state is known. The remainder of the paper is organized as follows. Section 2 introduces

186   the formulation, localization and inflation techniques of the 4DEnVar system. Section 3 follows

187   with the implementation of the 4DEnVar system and the experiment descriptions. Section 4

188   evaluates the performance of the 4DEnVar system on analyses and forecasts relative to the 4DVar

189   system. The summary and the prospect for future work are presented in the last section.

190   **2 Description of method**

191   2.1 Incremental 4DVar algorithm

192   The variational system used in this paper (Zhang et al, 2019) adopts the incremental 4DVar

193   scheme (Courtier et al., 1994), which usually obtains the optimal analysis of IC by minimizing a

194   cost function on a low-resolution grid:

$$J[\delta x(t_0)] = \frac{1}{2}\{\delta x(t_0) - [x^b(t_0) - x^g(t_0)]\}^T B_0^{-1}\{\delta x(t_0) - [x^b(t_0) - x^g(t_0)]\} + \frac{1}{2}\sum_{i=0}^{n}[\mathbf{H}_i\delta x(t_i) - d_i]^T R_i^{-1}[\mathbf{H}_i\delta x(t_i) - d_i], \tag{1}$$

195   where x^b is the background state vector, x^g is the first guess vector, $\delta x = x - x^g$ is the

196   perturbation of the IC, $\delta x(t_i) = \mathbf{M}_i\delta x(t_0)$ is the perturbation at time t_i, B is the static B-matrix,

197   and R is the observation error covariance matrix. $d_i = y_i^o - H_i[x^g(t_i)]$ contains the observation

198   innovations at time t_i, y_i^o contains the observations at time t_i, involving the observation operator

199   H_i at time t_i and the nonlinear forecast model integration M_i from the analysis time to time t_i. $\mathbf{H}_i$

200   is the tangent linear observation operator corresponding to H_i, and $\mathbf{M}_i$ is the TLM of M_i.

201   The convergence rate of the gradient for the optimization problem is dependent on the

202   condition number of the Hessian matrix (Zupanski, 1996). Operational DA systems generally

203   reduce the condition number of the Hessian matrix of Eq. (1) through the preconditioning

204   transformation, that is $\delta x = Uv$. Thus, the modeled climatological BEC can be estimated by

$$B_c = UU^T, \tag{2}$$

205 where v is the preconditioned state variable vector. U contains the physical transformation

206 operator that transforms independent variables to model variables, the diagonal matrix composed

207 of the background error variance square root of the independent variables, and the background

208 error correlation transformation matrix (Zhang et al., 2019). After the aforementioned

209 preconditioning transformation, Eq. (1) becomes

$$J[v(t_0)] = \frac{1}{2}[v(t_0)]^T[v(t_0)] + \frac{1}{2}\sum_{i=0}^{n}[\mathbf{H}_i\mathbf{M}_iUv(t_0) - d_i]^T R_i^{-1}[\mathbf{H}_i\mathbf{M}_iUv(t_0) - d_i]. \tag{3}$$

210 In order to minimize Eq. (3), the corresponding gradient should equal to zero, and the ADM

211 is required for calculating the gradient of the cost function. Moreover, the calculation of the ADM

212 requires the backward model trajectories, which are typically provided by the nonlinear forecast

213 model and expensive in calculation and storage. Thus, the adjoint-free DA method may be an

214 efficient alternative to 4DVar for operational applications.

215 2.2 4DEnVar

216 2.2.1 Algorithm

217 The 4DEnVar algorithm is based on the DRP-4DVar approach (Wang et al, 2010a) that

218 projects the initial increment δx in model space onto the subspace expanded by a limited number

219 of IC perturbation samples as its basis vectors, and obtains the optimal solution directly in the

220 subspace.

221 For the convenience of implementing 4DEnVar in the standard 4DVar framework, the IC

222 perturbation samples are obtained by the "randomcv" method, which uses the variational variable

223 transform $\delta x = Uv$ to produce an ensemble of balanced and reasonable perturbations (Baker,

224 2005). $X = [\delta x_1, \delta x_2, \cdots, \delta x_K]$ contains the IC perturbation samples, where K is the ensemble

225 size. The corresponding observational perturbation samples $Y = [\delta y_1, \delta y_2, \cdots, \delta y_K]$ are calculated

226 using TLMs and tangent linear observation operators. Thus, an ensemble of IC perturbation

227 samples and observational perturbation samples are chosen to define the following projection

228 matrices:

$$\begin{cases} p_x = \frac{1}{\sqrt{K-1}}[\delta x_1 - \overline{\delta x}, \delta x_2 - \overline{\delta x}, \cdots, \delta x_K - \overline{\delta x}] \\ p_y = \frac{1}{\sqrt{K-1}}[\delta y_1 - \overline{\delta y}, \delta y_2 - \overline{\delta y}, \cdots, \delta y_K - \overline{\delta y}] \end{cases}, \tag{4}$$

229   where $\begin{cases} \overline{\delta x} = \frac{1}{K}[\delta x_1 + \delta x_2 + \cdots + \delta x_K] \\ \overline{\delta y} = \frac{1}{K}[\delta y_1 + \delta y_2 + \cdots + \delta y_K] \end{cases}$. Defining $\alpha = (\alpha_1, \alpha_2, \cdots, \alpha_K)^T$ as a K-dimensional

230   vector composed of the weight coefficients of the basis vectors, δx and $\mathbf{H}_i \delta x(t_i)$ can be projected

231   onto the subspace spanned by the ensemble samples via the following transformation:

$$\begin{cases} \delta x = p_x \alpha \\ \mathbf{H}_i \delta x(t_i) = p_y(t_i)\alpha \end{cases}, \tag{5}$$

232   where $p_y(t_i)$ is the observational projection matrix at time t_i. Thus, the ensemble BEC can be

233   represented by

$$B_e = p_x p_x^T \tag{6}$$

234   and the new cost function with respect to α can be written as:

$$J[\alpha(t_0)] = \frac{1}{2}[\alpha(t_0)]^T[\alpha(t_0)] + \frac{1}{2}\sum_{i=0}^{n}[p_y(t_i)\alpha(t_0) - d_i]^T R_i^{-1}[p_y(t_i)\alpha(t_0) - d_i]. \tag{7}$$

235   To minimize Eq. (7), α must satisfy $\left[\frac{\partial J}{\partial \alpha(t_0)}\right]^T = 0$. Here, no ADM is needed. It is noted

236   that a degraded analysis may result from the approximation in Eq. (5) due to the much smaller

237   ensemble size than the dimension of the original IC perturbation, which can be alleviated by

238   localization techniques.

239   2.2.2 Localization

240   The major drawback to the ensemble-based method is its spurious correlations and very

241   small rank in the BEC due to the limited number of the IC perturbation samples, which excessively

242   constrains the solving subspace of the optimal analysis increment. Localization is considered to be

243   an effective technique to alleviate the aforementioned problems (Hamill et al., 2001).

244   The localized B-matrix can be typically expressed as the Schür product between the

245   ensemble BEC B_e and the correlation matrix of the covariance localization C. Because the direct

246   use of the localized B-matrix may lead to much computational cost according to Wang et al.

247   (2018), this matrix should be expressed in a form that can be used easily and economically. The

248   correlation matrix can be approximately decomposed into a limited number of leading

249   eigenvectors and extended IC perturbation samples can be obtained:

$$Ep_x = [(p_{x,1} \circ \boldsymbol{\rho}_{x,1}, \cdots, p_{x,1} \circ \boldsymbol{\rho}_{x,L}), \cdots, (p_{x,K} \circ \boldsymbol{\rho}_{x,1}, \cdots, p_{x,K} \circ \boldsymbol{\rho}_{x,L})], \qquad (8)$$

250   where $\boldsymbol{\rho}_{x,j}$ $(j = 1, 2, \cdots, L)$ is a leading eigenvector in model space, and L is the number of the

251   selected leading eigenvectors according to the cumulative contribution of variance. In

252   implementation, each leading eigenvector can be decomposed into zonal, meridional and vertical

253   components: $\boldsymbol{\rho}_{x,j} = \boldsymbol{\rho}^z_{x,j_z} \circ \boldsymbol{\rho}^m_{x,j_m} \circ \boldsymbol{\rho}^v_{x,j_v}$. The EOF decomposition method is used to obtain the

254   zonal and vertical components:

$$\begin{cases} \boldsymbol{\rho}^z_{x,j_z} = \boldsymbol{E}^z_{x,j_z} (\lambda^z_{x,j_z})^{1/2} \\ \boldsymbol{\rho}^v_{x,j_v} = \boldsymbol{E}^v_{x,j_v} (\lambda^v_{x,j_v})^{1/2} \end{cases}, \qquad (9)$$

255   where $\boldsymbol{E}^z_{x,j_z}$ and $\boldsymbol{E}^v_{x,j_v}$ are eigenvectors for the zonal and vertical components, respectively,

256   obtained using the empirical orthogonal decomposition. λ^z_{x,j_z} and λ^v_{x,j_v} are their corresponding

257   eigenvalues. Then, the sine expansion method is utilized (Wang et al., 2018) to obtain the

258   meridional component:

$$\boldsymbol{\rho}^m_{x,j_m} = \boldsymbol{E}^m_{x,j_m} \beta^{1/2}_{x,j_m} . \qquad (10)$$

259   Here, $\boldsymbol{E}^m_{x,j_m}$ is the eigenvector for the meridional component, and β_{x,j_m} is its eigenvalue. When

260   defining the correlation function model, we used the GC correlation function (Gaspari & Cohn,

261   1999) for the horizontal components:

$$C(r) = \begin{cases} -\dfrac{1}{4}r^5 + \dfrac{1}{2}r^4 + \dfrac{5}{8}r^3 - \dfrac{5}{3}r^2 + 1, 0 \le r \le 1 \\ \dfrac{1}{12}r^5 - \dfrac{1}{2}r^4 + \dfrac{5}{8}r^3 + \dfrac{5}{3}r^2 - 5r + 4 - \dfrac{2}{3}r^{-1}, 1 < r \le 2 \\ 0, 2 < r \end{cases} \qquad (11)$$

262   Here, r is defined as the dimensionless latitude and longitude distance. The following correlation

263   function is used for the vertical component:

$$C(r) = \frac{1}{1.0 + K_p r^2}. \qquad (12)$$

264 where r is defined as the dimensionless logarithmic pressure distance.

265 According to Eq. (8) and ignoring the time-variation of the localization leading
266 eigenvectors, the extended observational perturbation samples can be then represented as

$$Ep_y = [(p_{y,1} \circ \boldsymbol{\rho}_{y,1}, \cdots, p_{y,1} \circ \boldsymbol{\rho}_{y,L}), \cdots, (p_{y,K} \circ \boldsymbol{\rho}_{y,1}, \cdots, p_{y,K} \circ \boldsymbol{\rho}_{y,L})]. \quad (13)$$

267 Redefining the control variables as an $K \times L$-dimensional vector β, the analysis increment and
268 observational increment can be modified as

$$\begin{cases} \delta x = Ep_x \beta \\ \mathbf{H}_i \delta x(t_i) = Ep_y(t_i)\beta \end{cases} \quad (14)$$

269 Finally, the localized cost function is formulated on the extended sample space. In the generation
270 of the extended observational perturbation samples, the TLM is called for only K times. On one
271 hand, the ensemble size can be greatly increased from the original samples to the extended samples
272 without any additional computational cost for TLM calling, and the leading eigenvectors in both
273 the model and observation space can be pre-calculated according to the coordinates of the model
274 grid and observation locations. On the other hand, spurious correlations among the original
275 samples can be significantly eliminated, and the calculation accuracy of the cost function and its
276 gradient can be improved given that the extended samples have better independence from each
277 other than the original samples.

278 2.2.3 Inflation

279 The 4DEnVar system uses an inflation technique similar to the Relaxation-to-prior-
280 perturbations (RTPP; Zhang et al., 2004) to mitigate the filter divergence problem during the
281 assimilation cycle. Different from the RTPP, this inflation adopts random perturbations with
282 balance constraints from the static BEC of the standard 4DVar system.

283 60 random samples with balance constraints $(\delta x_k)_r$ $(k = 1, 2, \cdots, 60)$ are obtained by the
284 "randomcv" method introduced in Section 2.2.1 (Baker, 2005). They are linearly combined with
285 the 60 analysis increment samples $(\delta x_k)_a$ $(k = 1, 2, \cdots, 60)$ using the weights $\gamma_1 = 0.2$ for the
286 former and $\gamma_2 = 0.9$ for the latter to achieve the inflation of the ensemble BEC for the next
287 assimilation after a number of model integrations from the beginning to the end of the assimilation
288 window initialized by the inflated analysis increments $(\delta x_k)_a^{inf}$ $(k = 1, 2, \cdots, 60)$, where

$$\begin{cases} (\delta x_k)_a^{inf} = \gamma_1 (\delta x_k)_r + \gamma_2 (\delta x_k)_a \\ (\delta x_k)_f = M[x_b + (\delta x_k)_a^{inf}] \end{cases} \quad (k = 1, 2, \cdots, 60). \tag{15}$$

289 An obvious advantage of this inflation method is that it is convenient and easy to generate the

290 random samples with balance constraints directly through the preconditioning process of the

291 4DVar system. Moreover, the inflation technique implicitly incorporates the climatological BEC

292 into the ensemble BEC to construct the hybrid B-matrix, which can be represented by

$$(B_e)_{inf} = (p_x)_f (p_x)_f^T. \tag{16}$$

293 Here, $(p_x)_f = [(\delta x_1)_f, (\delta x_2)_f, \cdots, (\delta x_{60})_f]$ contains the updated inflated analysis increments.

294 Thus, the inflation method not only alleviates the underestimation of the B-matrix, but also

295 implicitly realizes the hybrid BEC for the 4DEnVar system.

296 **3 Experimental design**

297 3.1 Implementation of 4DEnVar system

298 In this study, the model used in the 4DEnVar system is the GRAPES-GFS model version

299 3.0 (Su et al., 2020) and contains 87 vertical levels. The horizontal resolution of the system is

300 $0.5° \times 0.5°$ for the outer loop and $1.0° \times 1.0°$ for the inner loop. The 4DEnVar system combines

301 the ensemble BEC estimated by 60 samples and the original variational framework to solve the

302 assimilation problem, and is evaluated in comparison to the available 4DVar system (Zhang et al,

303 2019) with the same model and same resolutions. The schematic flowchart in Figure 1 describes

304 the operational process of the 4DEnVar system. In order to mitigate the sampling errors and

305 spurious correlations in the BEC due to the limited ensemble size (Hamill et al., 2001; Lorenc et

306 al., 2003; Wang et al., 2010b, 2018), the localization scheme is designed according to the

307 implementation introduced in Section 2.2.2, with 7° for the filtering radius in the horizontal

308 direction and 3 for the filtering parameter K_p in the vertical direction. The minimization problem

309 of the 4DEnVar system is solved in the subspace spanned by the extended samples derived from

310 the Schür products between the ensemble members and the leading eigenvectors of the localization

311 correlation function. The 4DEnVar system not only can realize the implicit flow-dependence of

312 the BEC within the assimilation window like the standard 4DVar system, but also can achieve the

313 explicit flow-dependent BEC from one assimilation window to the next. During the assimilation

314   cycle, the perturbed observations are continuously assimilated into the ensemble samples, and the

315   flow-dependent ensemble samples are updated every 6 hours.

316   To alleviate the underestimation of the BEC in the assimilation cycle, an inflation

317   technique based on the random perturbations with balance constraints is applied. Collaborated with

318   the localization and perturbing techniques of observation and SST, the inflation may alleviate the

319   filtering divergence problem during the assimilation cycle. Observational perturbations are

320   obtained by superimposing normal distribution random perturbations with zero as their

321   expectations (or mean values) and the observation errors as their standard deviations onto the

322   observations. SST perturbations are produced similarly except that the standard deviations of

323   random perturbations adopts the SST analysis errors.

324   3.2 Experiment design

325   In order to evaluate the performance of the 4DEnVar system efficiently, the OSSE is

326   considered as one of the best choices. Here, two OSSEs are designed using the 0.25° × 0.25°

327   version of GRAPES-GFS for both the 4DEnVar and standard 4DVar systems. The OSSE for the

328   latter is to provide a reference for comparisons.

329   A previous study has demonstrated that the 4DVar system using the GRAPES-GFS model

330   significantly outperforms the 3DVar system using the same model on both analyses and medium-

331   range forecasts, especially in the Southern Hemisphere (Zhang et al., 2019). OSSEs can be used

332   to fairly evaluate the performance of the assimilation system (Wang et al., 2008a; Wang et al.,

333   2010a; Kleist et al., 2015a, 2015b). In order to further study the influence of the 4DEnVar system,

334   comparisons between it and the 4DVar system are necessary.

335   The time period of both experiments was about one month (0900 UTC 13 September 2016

336   - 0900 UTC 11 October 2016) after a 2-day assimilation cycle covering the period from 0900 UTC

337   11 September 2016 to 0900 UTC 13 September 2016 to alleviate the influence of the spin-up. Only

338   the inflation coefficient tuning experiments were analyzed for about one weak (0900 UTC 13

339   September 2016 - 0900 UTC 18 September 2016). The analysis time was taken at the beginning

340   of the assimilation window. In the OSSEs, the results from an uninterrupted free run with the

341   higher-resolution (0.25° × 0.25°) version of GRAPES-GFS were used as the "truth" state. To

342   eliminate the impact of spin-up, the "truth" state was initiated from the time 24 hours prior to the

343   analysis time of the first assimilation window with the ERA-5 reanalysis field as the IC, which
344   was verified to be consistent with the realistic atmospheric state in terms of geopotential height
345   and precipitation in the first 8 days. For example, we investigated the rationality of the "truth" state
346   in the Northern and Southern Extratropics based on a comparison of the 500hPa geopotential
347   height between the ERA-Interim reanalysis and the "truth" state at 1200 UTC on 14, 16 and 18
348   September 2016 (Figure 2). Figure 2a shows the 500hPa geopotential height from the ERA-Interim
349   reanalysis in the Northern Extratropics at 1200 UTC on 14 September 2016, with a low-pressure
350   system near the Arctic and 4 troughs extended from the low-pressure system near 60°E, 180°,
351   120°W and 30°W. The low-pressure system extends along 180° and 30°W, and the locations and
352   intensities of other main systems change slightly as the integration time increases (Figures 2e and
353   2i). The "truth" state captures these main features and their time-variations (Figures 2b, 2f and 2j).
354   Similarly, Figure 2c shows the results from the ERA-Interim reanalysis in the Southern
355   Extratropics. A low-pressure system exists near the Antarctic at 180° with 3 troughs near 0°, 90°W
356   and 90°E, and some troughs at low and middle latitudes. As the integration time increases, the
357   intensity of the low-pressure system near the Antarctic weakens and a high value center appears
358   near 60°E, and the locations and intensities of the main systems at low and middle latitudes change
359   slightly (Figures 2g and 2k). The "truth" state simulates these main systems well (Figures 2d, 2h
360   and 2l). In general, the "truth" state reasonably captures the main features and the time-variations
361   of the 500hPa geopotential height from the ERA-Interim reanalysis and gradually degrades
362   following the increase of integration time.

363   The "observations" were produced by interpolating the "truth" state to the positions at
364   which sounding and cloud-derived wind observations are located, and then superimposing normal
365   distribution random perturbations with zero as their expectations and the observation errors as their
366   standard deviations onto them. Figure 3 shows the spatial distribution of these observations.
367   Sounding observations are typically sampled in the continental areas of the Northern Extratropics
368   and are valid at 1200 UTC 13 September 2016. Cloud-derived wind observations are sampled
369   every 30 minutes, mainly in the central and eastern North Pacific, the eastern South Pacific, the
370   northern Indian Ocean, the Atlantic Ocean, as well as some continents such as the America and
371   Africa. The observation errors were taken the same as the 4DVar system.

372   For the first assimilation window of the 4DVar system, the background was obtained from

373   a 15-h forecast by the 0.5° × 0.5° version of GRAPES-GFS initialized from the 6-h forecast of the

374   ERA-Interim dataset, so that it is different from the "truth" state. Meanwhile, for the first

375   assimilation window of the 4DEnVar system, 60 IC samples were generated by superimposing 60

376   random perturbation samples onto this background. These perturbation samples were generated

377   according to the "randomcv" method introduced in Section 2.2.1 (Baker, 2005). The background

378   for each assimilation window of the 4DEnVar system is the ensemble mean of the IC samples of

379   this window, which are derived from 60 6-h forecasts by the 0.5° × 0.5° version of GRAPES-GFS

380   with 60 inflated analysis samples produced in the previous assimilation window as their ICs,

381   respectively, except for the first assimilation window. The 4DEnVar system has the same

382   background as the 4DVar system in the first assimilation window because the ensemble mean of

383   60 superimposed random perturbation samples is zero.

384   In addition, based on the OSSE for the 4DEnVar, two sets of SOEs were also conducted

385   for both the 4DEnVar and 4DVar systems within a 6-h window covered the period from 0900 UTC

386   13 September 2016 to 1500 UTC 13 September 2016 after a 2-day assimilation cycle to verify the

387   flow-dependent characteristic of the BECs. Both sets of SOEs adopted the same filtering radius

388   that is 15° in the horizontal direction and the same background that is the ensemble mean of the

389   IC samples produced by the 4DEnVar system. In each set of SOE, the DA system assimilated the

390   single-point observation valid at the beginning, middle and end of the assimilation window,

391   respectively. The first single-point observation valid at 1200 UTC 13 September (i.e., at the middle

392   of the window) was selected from the "observations" in the OSSEs, which is the single-point

393   temperature observation located upstream at the top of the short-wave ridge in the middle

394   troposphere, and the other two at the beginning and end of the window took the same location and

395   observation innovation as the first. The observation error was set to 0.95, and the observation

396   innovation was -1.53 K.

397   **4 Results**

398   4.1 Single-point observation experiments

399   Figures 4a and 4d show the analysis increments from the 4DVar and 4DEnVar systems,

400   respectively, which are produced by assimilating the same single-point temperature observation at

401 the beginning of the assimilation window in two SOEs. Both increments show the maximum

402 negative values near the observation as a response to the low temperature observation. The 4DVar

403 analysis increment of temperature appears a quasi-Gaussian distribution around the observation

404 location (Figure 4a). Given that the analysis time the resultant analysis increment is obtained is the

405 same as the time the single-point observation is located at, this distribution is reasonable. In

406 contrast, the 4DEnVar analysis increment of temperature, obtained using the ensemble BEC,

407 extends along the gradient of geopotential height, which is consistent with the northwestern

408 background flow. This visually demonstrates the explicit flow-dependence of the BEC of the

409 4DEnVar system. Furthermore, satisfactorily, no spurious correlations are sighted near the analysis

410 increment produced by the 4DEnVar system when the signal of the observation is preserved in the

411 analysis increment (Figure 4d). Both experiments also show cyclone wind responses around the

412 temperature increments, which suggests that the BECs satisfy some balance constraints. These

413 results are consistent with the SOEs introduced in Kleist et al. (2015b).

414 We further investigated the implicit flow-dependence of the BECs of both systems within

415 the assimilation window by visualizing the analysis increments obtained by assimilating single-

416 point observations valid at different time levels. Unlike those with the observation at the beginning

417 of the assimilation window, the maximum negative values of the increments produced by both

418 systems shift towards the northwest of the observation. Moreover, the further the observation is

419 located from the analysis time, the more the increments from both systems extend along the

420 gradient of geopotential height (Figures 4b, 4c, 4e and 4f). These suggest that 4DVar realized the

421 evolution of BEC within the assimilation window using the TLM and the ADM, while 4DEnVar

422 did through the statistical relationship between the model space and observation space.

423 4.2 Observing system simulation experiments

424 We divided the globe into four regions for the statistics and analysis of the following

425 indicators, including the Northern Extratropics (20°N~90°N, 180°W~180°E; NH-X), Southern

426 Extratropics (20°S~90°S, 180°W~180°E; SH-X), East Asia (15°N~65°N, 70°E~145°E; EA) and

427 Tropics (20°S~20°N, 180°W~180°E; TR). Considering that the root mean square error (RMSE)

428 mainly measures the random error that is not as correctable as the systematic bias, it is usually

429 applied to statistically analyze the random errors of the background and analysis fields. To exclude

430   the systematic error from the RMSE, we use a metrics called anomaly RMSE (ARMSE) instead

431   of RMSE (He et al. 2020a):

$$ARMSE = \sqrt{\frac{\sum_{n=1}^{N} w_{(n)} \times \left(M_{(n)} - truth_{(n)} - bias\right)^2}{\sum_{n=1}^{N} w_{(n)}}}. \qquad (17)$$

432   Here, $M_{(n)}$ and $truth_{(n)}$ represent the analysis (or background) and the "truth" state at the n-th

433   grid point, respectively. $w_{(n)}$ denotes the weighted coefficients at the n-th grid point, and $bias =$

434    $\frac{\sum_{n=1}^{N} w_{(n)} \times \left(M_{(n)} - truth_{(n)}\right)}{\sum_{n=1}^{N} w_{(n)}}$ represents the systematic bias.

435   4.2.1 Inflation impact

436   In order to study the impact of the inflation technique introduced in Section 2.2.3 on the

437   4DEnVar system, we compared the forecast skills of the experiments initialized by the 4DEnVar

438   system adopting different sets of inflation coefficients.

439   The inflation coefficients in the 4DEnVar system were set to be larger for the ensemble

440   analyses than for the random perturbations with balance constraints, so that a significant reduction

441   of the flow-dependent characteristic of the ensemble covariance was avoided during the

442   assimilation cycle. We tested several sets of inflation coefficients, including $(0.1, 1.0)$, $(0.2, 0.9)$,

443    $(0.3, 0.8)$ and $(0.5, 0.6)$, where the first and second numbers in the parentheses are the coefficients

444   for the random perturbations and ensemble analyses, respectively, and the results of the overall

445   scores of the experiments were given in Figure 5. The scorecard shows that the 4DEnVar system

446   using the inflation coefficient of $(0.2, 0.9)$ has the best performance in reducing ARMSE of the

447   forecast initialized from the ensemble mean analysis than those of tests using other sets of inflation

448   coefficients. A proper inflation improve the ensemble spread, but too strong inflation may lead to

449   excessive spread of some variables in the ensemble. These suggest that the inflation technique can

450   help the 4DEnVar system reduce the forecast errors.

451   4.2.2 Analysis error

452   To facilitate comparisons with reanalysis data that are located at the middle of the

453   assimilation window, all background and analysis fields from both DA systems are transformed

454   from the beginning to the middle of the window through 3-h forecasts using the $0.5° \times 0.5°$

455   version of GRAPES-GFS, which is similar to Zhang et al. (2019). Figure 6 shows the vertical

456   profiles of the ARMSEs of the background and analysis fields from the 4DVar and 4DEnVar

457   systems relative to the "truth" state. On one hand, comparing with the background fields, the

458   analysis fields from both assimilation approaches basically improve most variables at most vertical

459   levels. These analyses significantly reduce the ARMSE of zonal wind at almost all vertical levels

460   in the Northern Extratropics, Southern Extratropics, East Asia and Tropics (Figures 6a-6d). No

461   significant differences of temperature between the backgrounds and analyses can be observed

462   (Figures 6e-6h) except that the 4DEnVar system improves the temperature in the middle and

463   higher troposphere in the Southern Extratropics (Figure 6f) and the temperatures from the analyses

464   in the lower troposphere in the East Asia by both the 4DEnVar and 4DVar systems are obviously

465   degraded (Figure 6g). As for the specific humidity, no distinct changes from the backgrounds to

466   analyses can be found except the degradations near the surface by both assimilation approaches

467   (Figures 6i-6l). On the other hand, 4DEnVar fully outperforms 4DVar on the backgrounds and

468   analyses of zonal wind, temperature and specific humidity in the aforementioned four regions.

469   4DEnVar makes the biggest improvement in zonal wind (temperature) in the stratosphere in the

470   East Asian (Tropics) relative to 4DVar (Figures 6c and 6h). Significant improvements in specific

471   humidity by 4DEnVar are mainly in the lower troposphere comparing with 4DVar.

472   The analysis error structures of the 4DEnVar and 4DVar experiments are very similar

473   (Figure 7 left and middle), which are also consistent with the analysis error structures of the 3DVar

474   experiment and the corresponding 3D hybrid assimilation experiment in Kleist et al. (2015a). As

475   shown in Figures 7a-7b, the zonal wind error maxima are distributed in the middle and upper

476   troposphere at middle latitudes in the Southern Extratropics, and large zonal wind errors even

477   extend to the lower troposphere near 60 °S. Compared with 4DVar, 4DEnVar reduces the analysis

478   errors of zonal wind mainly at the latitudes between 60°S and 60°N, although it increases the

479   analysis errors in the middle and higher troposphere at high latitudes in the Northern Extratropics

480   and the analysis errors in the stratosphere at middle and high latitudes in the Southern Extratropics

481   (Figure 7c). Large temperature errors in the analyses of both assimilation approaches are

482   concentrated in the lower troposphere, especially in the region from the Antarctica to 60°S, which

483   extend to the middle and upper troposphere near 60°S (Figures 7d-7e). 4DEnVar has smaller

484   ARMSEs of temperature than 4DVar over most latitudes except for lower troposphere at high

485   latitudes and stratosphere at the latitudes around 60°S in the Southern Extratropics (Figure 7f).

486   Specific humidity shows analysis error structures quite different from the zonal wind and

487   temperature, which have semicircular shapes located between 60°S and 60°N in the lower and

488   middle troposphere (Figures 7g-7h). In the regions large humidity errors locate at, 4DEnVar

489   improves the accuracies of almost all humidity analyses (Figure 7i). In a word, 4DEnVar reduces

490   most analysis errors of zonal wind, temperature and specific humidity in comparison to 4DVar.

491   4.2.3 Forecast skill

492   From the above discussions, it can be found that the analysis accuracy of the 4DEnVar

493   system is basically higher than that of the 4DVar system. Based on these encouraging results, our

494   attention is now drawn to the impact of these more realistic analysis ICs on the forecasts. We want

495   to know whether the improved analysis IC can lead to improved forecasts. For this reason, the

496   analysis fields at 0900 UTC covered the period from 0900 UTC 13 September 2016 to 0900 UTC

497   11 October 2016 produced by the 4DEnVar and 4DVar systems were used as ICs to conduct a set

498   of 10-day forecasts. Similar to the analyses that were extended to the middle of the assimilation

499   window for evaluation, these forecasts with 3-hour extension for each lead forecast day were used

500   for evaluation. Because the 4DEnVar is an ensemble-based assimilation approach that produced

501   60 analysis ICs in the OSSE, 60 sets of 10-day forecasts were obtained using these analysis ICs.

502   For convenience of comparing with the single set of 10-day forecast initialized from the 4DVar

503   analysis, the ensemble mean 10-day forecast initialized from the 60 sets of 4DEnVar analyses was

504   used. Also, for a more comprehensive comparison with 4DVar, the results of the deterministic

505   forecast initialized from the 4DEnVar ensemble mean analysis were given. The forecasts were

506   evaluated using the "truth" state as the reference and adopting the anomaly correlation coefficient

507   (ACC) and ARMSE as the metrics.

508   ACC is one of the important metrics to investigate the skill of a forecast, which is used to

509   qualitatively measure the similarity between the anomalies of this forecast and the "truth" state. In

510   terms of this metrics, the 4DEnVar-based 10-day deterministic and ensemble mean forecasts of

511   500hPa geopotential height have comparable skills to and higher skills than the 4DVar-based

512   forecast on most lead forecast days, respectively (Figure 8). In the Northern Extratropics, the

513   4DEnVar-based deterministic and 4DVar-based forecasts have comparable skills on the lead days

514   1-5, and the former has slightly higher skills on the lead days 6-8 and slightly lower skills on the

515   lead days 9-10 (Figure 8a). In contrast, in the Southern Extratropics (Figure 8b), where

516   observations are much sparser than in the Northern Extratropics (Figure 3), the former has skills

517   comparable to or even slightly lower than the latter on the first 6 lead days and slightly higher

518   skills than the latter on the lead days 7-10. Similar to the Northern Extratropics, the 4DEnVar-

519   based deterministic forecast has comparable or even slightly higher skills on the lead days 1-7, but

520   slightly lower skills on the lead days 8-10 in the East Asia (Figure 8c). In the Tropics, the

521   4DEnVar-based deterministic forecast has lower skills on the first 5 lead days, and slightly higher

522   skills on the lead days 6-10 than the 4DVar-based forecast (Figure 8d). In comparison, the

523   4DEnVar-based ensemble mean forecast has significantly higher forecast skills on almost all lead

524   forecast days than the 4DEnVar-based deterministic and 4DVar-based forecasts (Figures 8a-8d).

525   In particular, the most significant improvements on the last few days in the Southern Extratropics

526   can be easily sighted in the 4DEnVar-based ensemble mean forecast comparing with the 4DVar-

527   based forecast. In summary, more accurate ICs from 4DEnVar generally achieve to higher forecast

528   skills in the ensemble mean forecast on almost all lead days than those from 4DVar in the single

529   forecast.

530   ARMSE is also an indispensable metrics to evaluate the skill of a forecast, which is used

531   to quantitatively measure the difference between the anomalies of this forecast and the "truth"

532   state. To facilitate the comparison between 4DEnVar and 4DVar on their contributions to forecast

533   skill, the difference of ARMSE between 4DEnVar and 4DVar is used, on which the confidence

534   test is conducted. The difference of ARMSE with a negative (positive) value indicates a further

535   improvement (degradation) of the forecast by 4DEnVar comparing with that by 4DVar. Figure 9

536   shows the differences of ARMSE of the 500hPa geopotential height forecasts between 4DEnVar

537   and 4DVar. The skill of the 4DEnVar-based forecast under this metrics basically matches that

538   under the metrics of ACC, i.e., the 4DEnVar-based deterministic and ensemble mean forecasts

539   have comparable performance to and better performance than the 4DVar-based forecast on most

540   lead days, respectively. This deterministic forecast has a performance comparable to or even better

541   than the 4DVar-based forecast on the first 9 lead days (the first 7 lead days), while the errors are

542   larger on the last 1 lead day (the last 3 lead days) in the Northern Extratropics (East Asia) as shown

543   in Figures 9a and 9c. In contrast, the former has larger errors on the first 6 lead days (the first 4

544   lead days) and smaller errors on the last few days than the latter in the Southern Extratropics

545   (Tropics) from Figures 9b and 9d. In addition, the 4DEnVar-based ensemble mean forecast reduce

546   errors significantly relative to the two abovementioned deterministic forecasts on almost all lead

547   days. In particular, the most significant improvements by the 4DEnVar-based ensemble mean

548   forecast relative to the 4DVar-based forecast can be sighted on the last few lead days in the

549   Southern Extratropics (Figure 9b), suggesting that the analysis ICs from the 4DEnVar system may

550   have much better capability to reduce the forecast errors of 500hPa geopotential height in the

551   regions with sparse observations. Due to the maximum improvements by 4DEnVar in the

552   ensemble mean forecast of the 500hPa geopotential height on the lead day 10 in both the Northern

553   and Southern Extratropics comparing with the 4DVar-based forecast (Figures 8a-8b and 9a-9b),

554   the horizontal distributions of the forecasts on this lead day were also analyzed and compared.

555   Figure 10 shows the "truth" state and the 240-h forecasts of the 500hPa geopotential height

556   respectively initialized from the 4DVar and 4DEnVar analyses on 1200 UTC 13 September 2016

557   in the Northern Extratropics. In the "truth" state, a low-pressure system is distributed around the

558   Arctic, with three troughs near 75°E, 160°W and 60°W, respectively. In addition, there is a high

559   value center at middle and high latitudes near the longitude 0° (Figure 10a). The main circulation

560   situations in the 4DVar-based (4DEnVar-based deterministic) forecast are basically similar to

561   those in the "truth" state (Figures 10b-10c), although the low-pressure trough (high value center)

562   near 160°W (the longitude 0°) is not correctly presented. Moreover, the main circulation situations

563   in the 4DEnVar-based ensemble mean forecast is similar to the 4DEnVar-based deterministic

564   forecast. As shown in Figure 10e, the 4DVar-based forecast has large errors with a "negative-

565   positive-negative" distribution between 90°W and 60°E at middle and high latitudes. It also

566   presents significant positive errors near 160°W at middle latitudes. In comparison, the 4DEnVar-

567   based deterministic forecast mainly reduces the magnitude of the errors in the regions between

568   90°E to 30°W at middle and high latitudes, especially the regions near 160°W and 40°W at middle

569   and high latitudes, but increases the errors in the regions between 30°W and 60°E at middle and

570   high latitudes, especially the regions near 30°E at high latitude (Figure 10f). In contrast, compared

571   with the 4DVar-based and 4DEnVar-based deterministic forecasts, the 4DEnVar-based ensemble

572   forecast significantly reduces errors in almost all regions, except the region between 30°E to 60°E.

573   Similar to Figure 10, Figure 11 shows the results in the Southern Extratropics. There is a low-

574   pressure system near the Antarctica, which extends out three troughs near 90°W, 150°E and 60°E,

575   respectively, in the "truth" state (Figure 11a). The 4DVar-based forecast and the 4DEnVar-based

576   deterministic and ensemble mean forecasts basically represent the circulation situations in the

577   "truth" state (Figures 11b-11d), but the first does not capture the troughs at 90°W very well. The

578 forecast errors of 4DVar in the Southern Extratropics are significantly larger than in the Northern

579 Extratropics (Figure 11e), while the 4DEnVar-based deterministic forecast reduces almost all the

580 significant forecast errors of 4DVar except the regions between 90°E and 0° (Figure 11f). In

581 addition, the 4DEnVar-based ensemble mean forecast significantly reduces the errors compared

582 with the 4DVar-based and 4DEnVar-based deterministic forecasts (Figure 11g). Overall, in terms

583 of the 500hPa geopotential height forecast, the 4DEnVar-based deterministic forecast has

584 comparable performance to the 4DVar-based forecast in the Northern Extratropics and slightly

585 better performance than the 4DVar-based forecast in the Southern Extratropics. Moreover, the

586 4DEnVar-based ensemble mean forecast significantly reduce the errors, especially in the Southern

587 Extratropics, which is consistent with the conclusions obtained by the ACC and ARMSE metrics.

588   The 4DEnVar-based forecast of geopotential height also has similar performances at most

589 other vertical levels (Figure 12). The 4DVar-based forecast errors show the largest in the Southern

590 Extratropics, followed by the Northern Extratropics and East Asia, and the smallest in the Tropics.

591 In the Northern Extratropics, the 4DVar-based forecast has significant errors at the vertical levels

592 between 400hPa and 200hPa, which keeps increasing following the lead time and reaches the

593 maximum on the lead day 10. These errors gradually extend to lower and upper levels following

594 the lead time (Figures 12a, 12d, 12g and 12j). As shown in Figure 12b, the 4DEnVar-based

595 deterministic forecast has a similar error structure to the 4DVar-based forecast except for larger

596 errors in the stratosphere, which extends to the troposphere on the lead days 1 and 10, and smaller

597 errors in the lower stratosphere and middle troposphere on the lead days 5-8, which extends to the

598 lower troposphere on the lead days 7-8. The maximum improvements (degradations) by the

599 4DEnVar-based deterministic forecast comparing with 4DVar are located between 400hPa and

600 200hPa (above 100hPa) on the lead days 6-7 (the lead days 1-9). In the Southern Extratropics, the

601 4DEnVar-based deterministic forecast has larger errors on the lead days 1-6 than the 4DVar-based

602 one, especially in the stratosphere on almost all lead days, and smaller errors on the last 3 lead

603 days (Figure 12e). In the East Asia, the 4DEnVar-based deterministic forecast has a performance

604 comparable to and even better than the 4DVar-based one on the lead days 1-7 except in the upper

605 stratosphere. However, it has larger errors on the last 3 lead days, especially between 600-100hPa

606 (Figure 10h). In the Tropics, it has a degradation near the stratosphere (the lower and middle

607 troposphere) on the lead days 1-9 (1-3) as shown in Figure 12k. In contrast, the 4DEnVar-based

608 ensemble mean forecast reduces errors at almost all regions and vertical levels on the middle and

609   later lead days compared with the 4DVar-based forecast, especially on the later days in the

610   Northern and Southern Extratropics, where the errors of the 4DVar-based forecast are the largest.

611   The places where the 4DEnVar-based deterministic forecast becomes worse than the 4DVar-based

612   forecast are largely improved in the ensemble mean forecast, especially for the lead days 8-10 in

613   the East Asia (Figures 12c, 12f, 12i and 12l).

614   The 4DVar-based zonal wind forecast has an error structure similar to the geopotential

615   height forecast at most vertical levels with the largest errors in the Southern Extratropics and

616   smallest errors in the Tropics (Figures 13a, 13d, 13g and 13j). The improvement and degradation

617   locations of the 4DEnVar-based deterministic forecast compared with the 4DVar-based forecast

618   are generally consistent with the geopotential height forecast (Figures 13b, 13e, 13h and 13k).

619   However, quite different from the geopotential height forecast, the 4DEnVar-based deterministic

620   forecast of zonal wind reduces the errors relative to the 4DVar-based forecast at almost all vertical

621   levels on the first lead day and the improvement extends to the lead day 9 (the lead day 7) in the

622   middle and upper troposphere of the Northern Extratropics (East Asia) as shown in Figure 13b,

623   13e, 13h and 13k. In contrast, the 4DEnVar-based ensemble mean forecast performs better in

624   almost all situations than the 4DVar-based forecast, especially on the middle and later lead days

625   (Figures 13c, 13f, 13i and 13l). In addition, the locations where the 4DEnVar-based deterministic

626   forecast deteriorates compared with 4DVar largely get improved in the 4DEnVar-based ensemble

627   mean forecast, especially for the lead days 2-7 in the Southern Extratropics and the lead days 8-10

628   in the East Asia (Figures 13f and 13i). However, the 4DEnVar-based ensemble mean forecast is

629   still worse than the 4DVar-based forecast on the first 5 lead days around the stratosphere in the

630   Southern Extratropics and Tropics, which is similar to the geopotential height forecast (Figures

631   12f and 12l).

632   The error distribution of the 4DVar-based temperature forecast is not quite the same as

633   those of the geopotential height and zonal wind forecasts, with the error size sorting as same as in

634   geopotential height and zonal wind forecasts (Figures 14a, 14d, 14g and 14j). The locations of the

635   improvements and degradations in the 4DEnVar-based deterministic temperature forecast relative

636   to the 4DVar-based forecast is similar to the zonal wind forecast but with the following differences.

637   The locations of the largest improvements in the 4DEnVar-based deterministic forecast in the

638   Southern Extratropics and East Asia compared with the 4DVar-based forecast extend to the lower

639   and middle troposphere. In addition, the ranges of the degradations of the 4DEnVar-based

640 deterministic forecast compared with the 4DVar-based forecast also increase (Figures 14b, 14e,

641 14h and 14k). In contrast, the 4DEnVar-based ensemble mean forecast is still significantly

642 improved for almost all situations compared with 4DVar (Figures 14c, 14f, 14i and 14l).

643 The 4DVar-based specific humidity forecast has an error structure different from other

644 variables, with large errors between 900hPa and 700hPa in each of four regions, increasing with

645 the lead time and reaching a maximum since the lead day 9 (Figures 15a, 15d, 15g and 15j).

646 Compared with the 4DVar-based forecast, the 4DEnVar-based deterministic forecast reduces

647 errors on the lead days 1-7 in the Northern Extratropics and East Asia, while degradation occurs

648 on the lead days 8-10 (Figures 15b and 15h). The 4DEnVar-based deterministic forecast reduces

649 errors in the Southern Extratropics (Tropics) except the lead days 3-7 (4-10) compared with 4DVar

650 (Figures 15e and 15k). In contrast, 4DEnVar-based ensemble mean forecast stably reduces errors

651 for almost all regions and lead days, and the largest improvements can be found where and when

652 large forecast errors of 4DVar are located (Figures 15c, 15f, 15i and 15l) .

653 4.2.4 Computational efficiency

654 The computational efficiency of the 4DEnVar system is also a key concern. Taking the 6-

655 h assimilation window (0900 UTC 11 September 2016 - 1500 UTC 11 September 2016) as an

656 example, the computational time was about 25 minutes for a 4DVar DA using 480 cores on the

657 high-performance computer PI-SUGON of the China Meteorological Administration. In

658 comparison, the 4DEnVar system took only 13 minutes since the ensemble members of the

659 4DEnVar system are independent and all members can be analyzed concurrently using a total of

660 60×480 cores. The aforementioned results may be slightly impacted by several factors, such as

661 the high-performance computer state, but overall, the 4DEnVar system has the advantage of good

662 parallel efficiency and scalability and is thereby timesaving when more computational resources

663 are used.

664 **5 Summary and discussion**

665 In this study, a new 4DEnVar DA system was developed based on the DRP-4DVar

666 approach. This system is novel in some aspects. It introduces the idea of ensemble into the

667 variational framework to achieve the time-variant BEC and minimizes the cost function without

668 using the ADM. It can easily take full advantage of the mature variational framework and

669 implicitly include the hybrid BEC into the pure ensemble covariance. An inflation method similar

670 to RTPP (Zhang et al., 2004) based on balanced random perturbations produced using the static

671 B-matrix of 4DVar is applied to alleviate the filter divergence during the assimilation cycle, which

672 can be conveniently and efficiently implemented. Moreover, a limited number of leading

673 eigenvectors of the localization correlation function are used to perform the localization of the B-

674 matrix and rapidly increase the ensemble size without any extra model integrations.

675 Preliminary tests including SOEs and OSSEs were conducted to evaluate the performance

676 of the 4DEnVar system, using the 4DVar system as a reference for comparison. The OSSE-based

677 one-month DA cycles using both systems were conducted, in which the first 2-day cycles were

678 used for spin-up. The SOEs were conducted at and the OSSE results were evaluated and compared

679 since the ninth assimilation window. The SOEs show that both 4DEnVar and 4DVar assimilated

680 the single-point observation effectively and satisfied certain balance constraints. Moreover,

681 4DEnVar using the ensemble BEC exhibits obvious flow-dependent features.

682 In the OSSEs, we first tuned the inflation coefficients. The weight of the ensemble analyses

683 kept larger than that of the balanced random perturbations to avoid too much loss of flow-

684 dependent information during the assimilation cycle. It is found that the forecast errors grow when

685 the inflation is too weak or too strong. Finally, the weights 0.9 for the ensemble analysis and 0.2

686 for the balanced random perturbations were thought to be the proper inflation coefficients, which

687 optimally reduced the ARMSEs of the forecast initialized by the 4DEnVar ensemble mean analysis.

688 The results of the OSSE-based one-month DA cycle show that the 4DEnVar and 4DVar

689 analyses can significantly improve the dynamic variables such as the zonal wind, and has slight

690 impacts on the thermodynamic variables such as the temperature and specific humidity compared

691 with their backgrounds. In addition, 4DEnVar outperforms 4DVar in terms of ARMSE on the

692 background and analysis fields of model variables. Compared with the 4DVar analysis, the

693 4DEnVar analysis can significantly reduce the errors in the model variables at low and middle

694 latitudes. The greatest improvements in the zonal wind and temperature by the 4DEnVar analysis

695 located mainly near the stratosphere, although there is significant degradation at high latitudes in

696 the Southern Extratropics. The greatest improvements in the specific humidity are mainly in the

697 lower troposphere. In conclusion, the analysis error of the 4DEnVar system is basically smaller

698 than that of the 4DVar system.

699   The effect of the 4DEnVar system on the forecast is also evaluated. From the ACC and

700   ARSME indicators of the 500hPa geopotential height forecasts, the 4DEnVar-based deterministic

701   forecast has a performance comparable to or slightly better than the 4DVar-based forecast in the

702   short and medium range in the Northern Extratropics and East Asia, and slightly worse

703   performance in the long range. In the Southern Extratropics and Tropics, the results are roughly

704   opposite to those in the Northern Extratropics and East Asia. Moreover, the 4DEnVar-based

705   ensemble mean forecast is comparable to or even better than the 4DVar-based forecast except for

706   the first few days in the Tropics. The geopotential height forecasts at other vertical levels are

707   generally consistent with the results of the 500hPa geopotential height, but both the deterministic

708   and ensemble mean forecasts from the 4DEnVar system show significant degradations near the

709   stratosphere.

710   The 4DEnVar-based deterministic forecasts of the zonal wind and temperature are similar

711   to and better than that of the geopotential height. In particular, these deterministic forecasts

712   outperform the 4DVar-based forecasts in almost all regions and vertical levels on the first lead day,

713   and this positive effect continues in the upper troposphere in the Northern Extratropics and East

714   Asia to the middle and later lead days, but the temperature forecasts are slightly worse than the

715   zonal wind. The improvements of the 4DEnVar-based deterministic specific humidity forecast

716   over the 4DVar-based one are mainly located on the early lead days. In contrast, the 4DEnVar-

717   based ensemble mean forecast of the zonal wind, temperature and specific humidity show

718   significant improvements over both the 4DVar and 4DEnVar-based deterministic forecasts, with

719   the greatest improvements on the later lead days.

720   Overall, the 4DEnVar system shows great promise in terms of reducing the analysis errors

721   and producing high quality ensemble forecasts. The significantly improved ensemble forecasts

722   from the 4DEnVar system suggest that they have the potential to provide high quality flow-

723   dependent ensemble BECs for hybrid DA systems. Moreover, 4DEnVar is more timesaving than

724   4DVar given that the ensemble members of 4DEnVar can be predicted and analyzed concurrently.

725   There is still much room for further improving the performance of the 4DEnVar system. For

726   example, the current localization used here does not include the balance constraints and a balanced

727   localization calls for further study. The localization length-scales currently adopted in the

728   4DEnVar system are constant and adaptive length-scales are expected in the future. The current

729   4DEnVar system borrows the low-resolution TLM of the 4DVar system and the NLM with the

730 same resolution may provide more accurate and more timesaving ensemble forecasts. In addition,

731 assimilation experiments using real observations, especially satellite radiance observations, should

732 be further carried out to evaluate the performance of the 4DEnVar system.

References

745 Barker, D. M. (2005). Southern high-latitude ensemble data assimilation in the Antarctic

746   mesoscale prediction system. *Monthly Weather Review, 133*(12), 3431-3449.

747 Bishop, C. H., Hodyss, D., Steinle, P., Sims, H., Clayton, A. M., Lorenc, A. C., Barker, D. M., &

748   Buehner, M. (2011). Efficient ensemble covariance localization in variational data assimilation.

749   *Monthly Weather Review, 139*, 573-580.

750 Bonavita, M., Isaksen, L., & Hólm, E. (2012). On the use of EDA background error variances in

751   the ECMWF 4D-Var. *Quarterly Journal of the Royal Meteorological Society, 138*(667), 1540-

752   1559.

753 Bowler, N. E., Clayton, A. M., Jardak, M., Jermey, P. M., Lorenc, A. C., Wlasak, M. A., Barker,

754   D. M., Inverarity, G. W., & Swinbank, R. (2017a). The effect of improved ensemble

755   covariances on hybrid variational data assimilation. *Quarterly Journal of the Royal*

756   *Meteorological Society, 143*: 785-797.

757 Bowler, N. E., Clayton, A. M., Jardak, M., Lee, E., Lorenc, A. C. and Piccolo, C., Pring, S. R.,
758   Wlasak, M. A., Barker, D. M., Inverarity, G. W., & Swinbank, R. (2017b). Inflation and
759   localization tests in the development of an ensemble of 4D-ensemble variational assimilations.
760   *Quarterly Journal of the Royal Meteorological Society, 143*(704): 1280-1302.

761 Buehner, M., Houtekamer, P. L., Charette, C., Mitchell, H. L., & He, B. (2010a). Intercomparison
762   of variational data assimilation and the ensemble Kalman filter for global deterministic NWP.
763   Part I: Description and single-observation experiments. *Monthly Weather Review, 138*(5),
764   1550-1566.

765 Buehner, M., Houtekamer, P. L., Charette, C., Mitchell, H. L., & He, B. (2010b). Intercomparison
766   of variational data assimilation and the ensemble Kalman filter for global deterministic NWP.
767   Part II: One-month experiments with real observations. *Monthly Weather Review, 138*(5),
768   1567-1586.

769 Buehner, M., Morneau, J., & Charette, C. (2013). Four-dimensional ensemble-variational data
770   assimilation for global deterministic weather prediction. *Nonlinear Processes in Geophysics,
771   20*(5), 669-682.

772 Buehner, M., Mctaggart-Cowan, R., Beaulne, A., Charette, C., Garand, L., Heilliette, S., Lapalme,
773   E., Laroche, S., Macpherson, S. R., Morneau, J., & Zadra, A. (2015). Intercomparison of
774   deterministic weather forecasting systems based on ensemble–variational data assimilation at
775   Environment Canada. Part I: The global system. *Monthly Weather Review, 143*, 2532-2559.

776 Chen, D. H., Xue, J. S., Yang, X. S., Zhang, H. L., Shen, X. S., Hu, J. L., Wang, Y., Ji, L. R., &
777   Chen, J. B. (2008). New generation of multi-scale NWP system (GRAPES): general scientific
778   design. *Chinese Science Bulletin, 53*(22), 3433–3445.

779 Clayton, A. M., Lorenc, A. C., & Barker, D. M. (2013). Operational implementation of a hybrid
780   ensemble/4D-Var global data assimilation system at the Met Office. *Quarterly Journal of the
781   Royal Meteorological Society, 139*(675), 1445-1461.

782 Courtier, P., Thépaut, J. N., & Hollingsworth, A. (1994). A strategy for operational implementation
783   of 4D-Var, using an incremental approach. *Quarterly Journal of the Royal Meteorological
784   Society, 120*(519), 1367-1387.

785   Evensen, G. (1994). Sequential data assimilation with a nonlinear quasi-geostrophic model using

786   Monte Carlo methods to forecast error statistics. *Journal of Geophysical Research*

787   *Oceans, 99*(C5), 10143–10162.

788   Evensen, G. (2003). The ensemble Kalman filter: Theoretical formulation and practical

789   implementation. *Ocean Dynamics, 53*(4), 343-367.

790   Gaspari, G., & Cohn, S. E. (1999). Construction of correlation functions in two and three

791   dimensions. *Quarterly Journal of the Royal Meteorological Society, 125*(554), 723-757.

792   Gauthier, P., & Thépaut, J. N. (2001). Impact of the digital filter as a weak constraint in the

793   preoperational 4dvar assimilation system of Météo-France. *Monthly Weather Review, 129*(8),

794   2089-2102.

795   Gauthier, P., Tanguay, M., Laroche, S., & Pellerin, S. (2007). Extension of 3dvar to 4dvar:

796   Implementation of 4dvar at the meteorological service of Canada. *Monthly Weather*

797   *Review, 135*(6), 2339-2354.

798   Hamill, T. M., & Snyder, C. (2000). A hybrid ensemble Kalman filter–3d variational analysis

799   scheme. *Monthly Weather Review, 128*(8), 2905-2919.

800   Hamill, T. M., Whitaker, J. S., & Snyder, C. (2001). Distance-dependent filtering of background

801   error covariance estimates in an ensemble Kalman filter. *Monthly Weather Review, 129*(11),

802   2776-2790.

803   He, Y., Wang, B., Liu, M., Liu, L., Yu, Y., Liu, J., Li, R., Zhang, C., Xu, S., Huang, W., Liu, Q.,

804   Wang, Y., & Li, F. (2017). Reduction of initial shock in decadal predictions using a new

805   initialization   strategy. *Geophysical   Research   Letters, 44*(16),   8538-8547,   DOI:

806   10.1002/2017GL074028.

807   He, Y., Wang, B., Liu, L., Huang, W., Xu, S., Liu, J., Wang, Y., Li, L., Huang, X., Peng, Y., Lin,

808   Y., & Yu, Y. (2020a). A DRP-4DVar-based coupled data assimilation system with a simplified

809   off-line localization technique for decadal predictions. *Journal of Advances in Modeling Earth*

810   *Systems, 12*, e2019MS001768. https://doi.org/10.1029/2019MS001768.

811   He, Y., Wang, B., Huang, W., Xu, S., Wang, Y., Liu, L., Li, L., Liu, J., Yu, Y., Lin, Y., Huang,

812   X., & Peng, Y. (2020b). A new DRP-4DVar-based coupled data assimilation system for

813   decadal predictions using a fast online localization technique. *Climate Dynamics, 54*(19), 3541-
814   3559, DOI: 10.1007/s00382-020-05190-w.

815   Houtekamer, P. L., Mitchell, H. L., Pellerin, G., Buehner, M., Charron, M., Spacek, L., & Hansen,
816   B. (2005). Atmospheric data assimilation with an ensemble Kalman filter: Results with real
817   observations. *Monthly Weather Review, 133*(3), 604-620.

818   Kleist, D. T., & Ide, K. (2015a). An OSSE-based evaluation of hybrid variational-ensemble data
819   assimilation for the NCEP GFS. Part I: System description and 3D-hybrid results. *Monthly*
820   *Weather Review, 143*, 433-451.

821   Kleist, D. T., & Ide, K. (2015b). An OSSE-based evaluation of hybrid variational–ensemble data
822   assimilation for the NCEP GFS. Part II: 4DEnVar and hybrid variants. *Monthly Weather*
823   *Review, 143*(2), 452-470.

824   Koizumi, K., Ishikawa, Y., & Tsuyuki, T. (2005). Assimilation of precipitation data to the JMA
825   mesoscale model with a four-dimensional variational method and its impact on precipitation
826   forecasts. *Sola, 1*, 45-48.

827   Kuhl, D. D., Rosmond, T. E., Bishop, C. H., Mclay, J., & Baker, N. L. (2013). Comparison of
828   hybrid ensemble/4dvar and 4dvar within the NAVDAS-AR data assimilation framework.
829   *Monthly Weather Review, 141*(8), 2740-2758.

830   Le Dimet, F. X., & Talagrand, O. (1986). Variational algorithms for analysis and assimilation of
831   meteorological observations: Theoretical aspects. *Tellus A: Dynamic Meteorology and*
832   *Oceanography, 38*(2), 97-110.

833   Lei, L., Whitaker, J. S., Anderson, J. L., & Tan, Z. (2020). Adaptive localization for satellite
834   radiance observations in an ensemble Kalman filter. *Journal of Advances in Modeling Earth*
835   *Systems, 12,* e2019MS001693. https://doi.org/ 10.1029/2019MS001693

836   Lewis, J. M., & Derber, J. C. (1985). The use of adjoint equations to solve a variational adjustment
837   problem with advective constraints. *Tellus A: Dynamic Meteorology and Oceanography, 37*(4),
838   309-322.

839   Li, F., Wang, B., He Y., et al. (2021a). Important role of North Atlantic air–sea coupling in the
840   interannual predictability of summer precipitation over the eastern Tibetan Plateau. *Climate*
841   *Dynamics, 56*, 1433-1448.

842   Li, F., Wang, B., He Y., et al. (2021b). Improved decadal predictions of East Asian summer
843   monsoon with a weakly coupled data assimilation scheme. *International Journal of*
844   *Climatology,* 1-22.

845   Liu, C., Xiao, Q., & Wang, B. (2008). An ensemble-based four-dimensional variational data
846   assimilation scheme. Part I: Technical formulation and preliminary test. *Monthly Weather*
847   *Review, 136*(9), 3363-3373.

848   Liu, C., Xiao, Q., & Wang, B. (2009). An ensemble-based four-dimensional variational data
849   assimilation scheme. Part II: Observing system simulation experiments with advanced research
850   WRF (ARW). *Monthly Weather Review, 137*(5), 1687-1704.

851   Liu, J., & Wang, B. (2011). Rainfall assimilation using a new four-dimensional variational method:
852   A single-point observation experiment. *Advances in Atmospheric Sciences, 28*(4), 735-742.

853   Lorenc, A. C. (2003). The potential of the ensemble Kalman filter for NWP—a comparison with
854   4D-Var. *Quarterly Journal of the Royal Meteorological Society, 129*(595), 3183-3203.

855   Lorenc, A. C., Bowler, N. E., Clayton, A. M., Pring, S. R., & Fairbairn, D. (2015). Comparison of
856   hybrid-4DEnVar and hybrid-4DVar data assimilation methods for global NWP. *Monthly*
857   *Weather Review, 143*(1), 212-229.

858   Qiu, C., Zhang, L., & Shao, A. (2007). An explicit four-dimensional variational data assimilation
859   method. *Science in China Series D: Earth Sciences, 50*(8), 1232-1240.

860   Rabier, F., Jarvinen, H., Klinker, E. Mahfouf J. F., & Simmons, A. (2000). The ECMWF
861   operational implementation of four-dimensional variational assimilation. I: Experimental
862   results with simplified physics. *Quarterly Journal of the Royal Meteorological*
863   *Society, 126*(564), 1143-1170.

864   Rawlins, F., Ballard, S. P., Bovis, K. J., Clayton, A. M., Li, D., Inverarity, G. W., Lorenc, A. C.,
865   & Payne, T. J. (2007). The Met Office global four-dimensional variational data assimilation
866   scheme. *Quarterly Journal of the Royal Meteorological Society, 133*(623), 347-362.

867   Raynaud, L., Berre, L., & Desroziers, G. (2011). An extended specification of flow-dependent
868   background error variances in the Météo-France global 4D-Var system. *Quarterly Journal of*
869   *the Royal Meteorological Society, 137*(656), 607-619.

870 Shen, S., Liu, J., & Wang, B. (2015). Evaluation of the historical sampling error for global models.
871   *Atmospheric and Oceanic Science Letters, 8*(5), 250–256.

872 Shi, P., Lu, H., Leung, L., He, Y., Wang, B., Yang, K., et al. (2021). Significant land contributions
873   to interannual predictability of East Asian summer monsoon rainfall. *Earth's Future, 9*, DOI:
874   10.1029/E2020EF001762.

875 Simmons, A. J., & Hollingsworth, A. (2002). Some aspects of the improvement in skill of
876   numerical weather prediction. *Quarterly Journal of the Royal Meteorological Society, 128*,
877   647-677.

878 Su, Y., Shen, X., zhang, H., & Liu, Y. (2020). A study on the three-dimensional reference
879   atmosphere in GRAPES_GFS: Constructive reference state and real forecast experiment (in
880   Chinese). *Acta Meteorologica Sinica, 78*(6):962-971. DOI: 10.11676/qxxb2020.075.

881 Tian, X., Xie, Z., & Dai, A. (2008). An ensemble-based explicit four-dimensional variational
882   assimilation method. *Journal of Geophysical Research: Atmospheres, 113*, D21124. DOI:
883   10.1029/2008JD010358

884 Tian, X., Xie, Z., and Sun, Q. (2011). A POD-based ensemble four-dimensional variational
885   assimilation method. *Tellus, 63A*(4), 805-816.

886 Wang, B., Liu, J. J., Wang, S., Cheng, W., Liu, J., Liu, C., Xiao, Q., & Kuo, Y. (2010a). An
887   economical approach to four-dimensional variational data assimilation. *Advances in*
888   *Atmospheric Sciences, 27*(4), 715-727.

889 Wang, B., Liu, J., Lu, B., & Tan, X. (2010b). An orthogonal expansion of filtering function in
890   localization and its application to solution of CNOP. *Geophysical Research Abstracts, 12*,
891   EGU2010-6786, EGU General Assembly 2010.

892 Wang, B., Liu, J., Liu, L, Xu, S., & Huang, W. (2018). An approach to localization for ensemble-
893   based data assimilation. *Plos One, 13*(1), e0191088. https://doi.org/10.1371/journal.
894   pone.0191088.

895 Wang, X., Barker, D. M., Snyder, C., & Hamill, T. M. (2008a). A hybrid ETKF-3DVAR data
896   assimilation scheme for the WRF model. Part I: Observing system simulation experiment.
897   *Monthly Weather Review, 136*(12), 5116-5131.

898 Wang, X., Barker, D. M. , Snyder, C., & Hamill, T. M. (2008b). A hybrid ETKF–3DVAR data
899   assimilation scheme for the WRF model. Part II: Real observation experiments. *Monthly*
900   *Weather Review, 136*(12), 5132-5147.

901 Wang, X., Parrish, D., Kleist, D., & Whitaker, J. (2013). GSI 3DVAR-based ensemble–variational
902   hybrid data assimilation for NCEP global forecast system: Single-resolution experiments.
903   *Monthly Weather Review, 141*(11), 4098-4117.

904 Wang, X., & Lei, T. (2014). GSI-based four-dimensional ensemble–variational (4DEnsVar) data
905   assimilation: Formulation and single-resolution experiments with real data for NCEP global
906   forecast system. *Monthly Weather Review, 142*(9), 3303-3325.

907 Whitaker, J. S., Hamill, T. M., Wei, X., Song Y., & Toth Z. (2008). Ensemble data assimilation
908   with the NCEP global forecast system. *Monthly Weather Review, 136*, 463-482.

909 Whitaker, J. S., Compo, G. P., & Thépaut, J. N. (2009). A comparison of variational and ensemble-
910   based data assimilation systems for reanalysis of sparse observations. *Monthly Weather*
911   *Review, 137*(6), 1991-1999.

912 Xue, J., Zhuang, S., Zhu, G., Zhang, H., Liu, Z., Liu, Y., & Zhuang, Z. (2008). Scientific design
913   and preliminary results of three-dimensional variational data assimilation system of GRAPES.
914   *Chinese Science Bulletin, 53*(22), 3446-3457.

915 Zhang, F. Q., Snyder, C., & Sun, J. (2004). Impacts of initial estimate and observation availability
916   on convective-scale data assimilation with an ensemble kalman filter. *Monthly Weather*
917   *Review, 132*, 1238-1253.

918 Zhang, L., Liu, Y. Z., Liu, Y., Gong, J., Lu, H., Jin, Z., Tian, W., Liu, G., Zhou, B., & Zhao, B.
919   (2019). The operational global four-dimensional variational data assimilation system at the
920   China Meteorological Administration. *Quarterly Journal of the Royal Meteorological Society,*
921   *145*, 1882–1896.

922 Zhang, M., & Zhang, F. (2012). E4dvar: Coupling an ensemble Kalman filter with four-
923   dimensional variational data assimilation in a limited-area weather prediction model. *Monthly*
924   *Weather Review, 140*(2), 587-600.

925 Zhao, J., & Wang, B. (2010). Sensitivity of the DRP-4DVar performance to perturbation samples
926   obtained by two different methods. *Journal of Meteorological Research, 24*(5), 527-538.

927   Zhao, Y., Wang, B., & Liu, J. J. (2012). A DRP-4DVar data assimilation scheme for typhoon
928   initialization using sea level pressure data. *Monthly Weather Review, 140*(4), 1191-1203.

929   Zupanski, M. (1996). A preconditioning algorithm for four-dimensional variational data
930   assimilation. *Monthly Weather Review, 124*(11), 2562-2573.

931
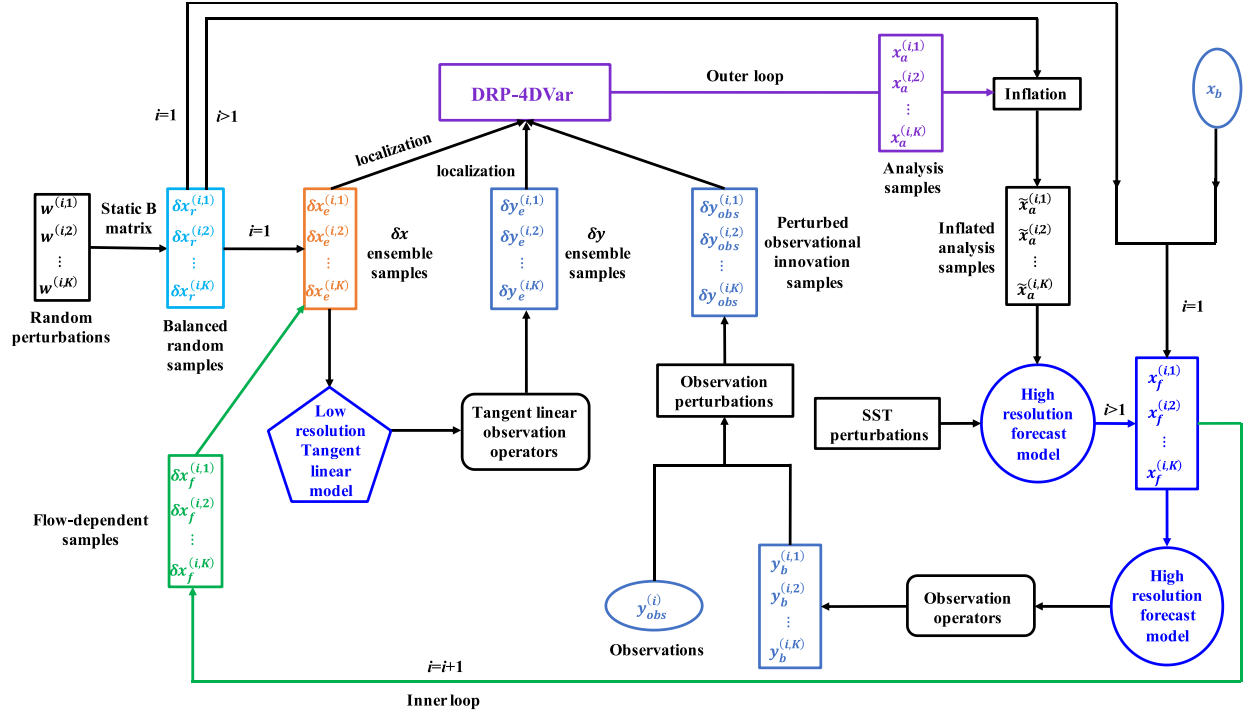
932 **Figure 1**. Schematic of the 4DEnVar system used in this study.
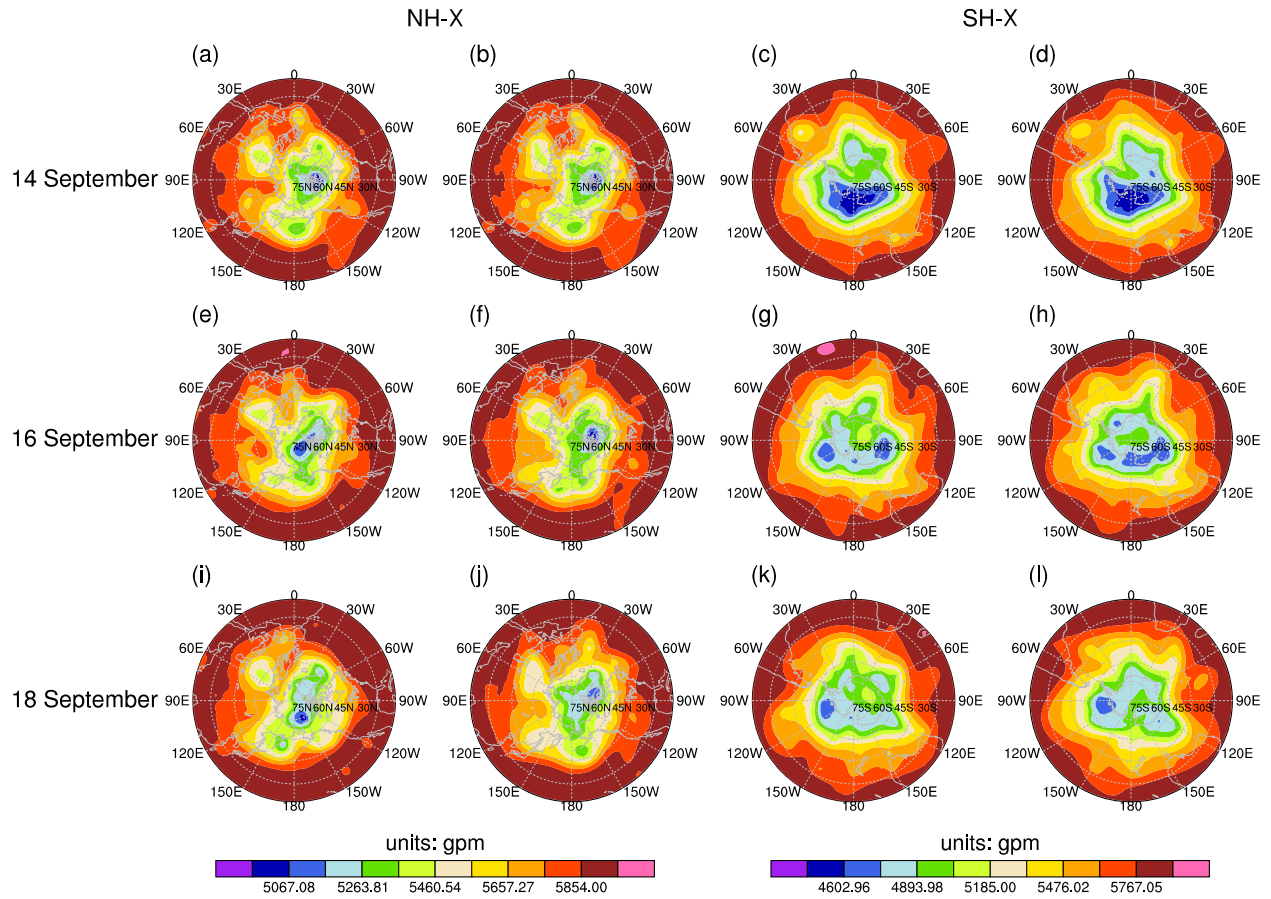
Figure 2. The 500hPa geopotential height at 1200 UTC on 14 September 2016 (top), 16 September 2016 (middle) and 18 September 2016 (bottom) from the ERA-Interim reanalysis (left) and the "truth" state (middle left) in the Northern Extratropics (20°N~90°N, 180°W~180°E), and the results in the Southern Extratropics (20°S~90°S, 180°W~180°E; the ERA-Interim reanalysis, middle right; the "truth" state, right) are plotted.

(a) Sounding locations

(b) Cloud-derived wind locations

939
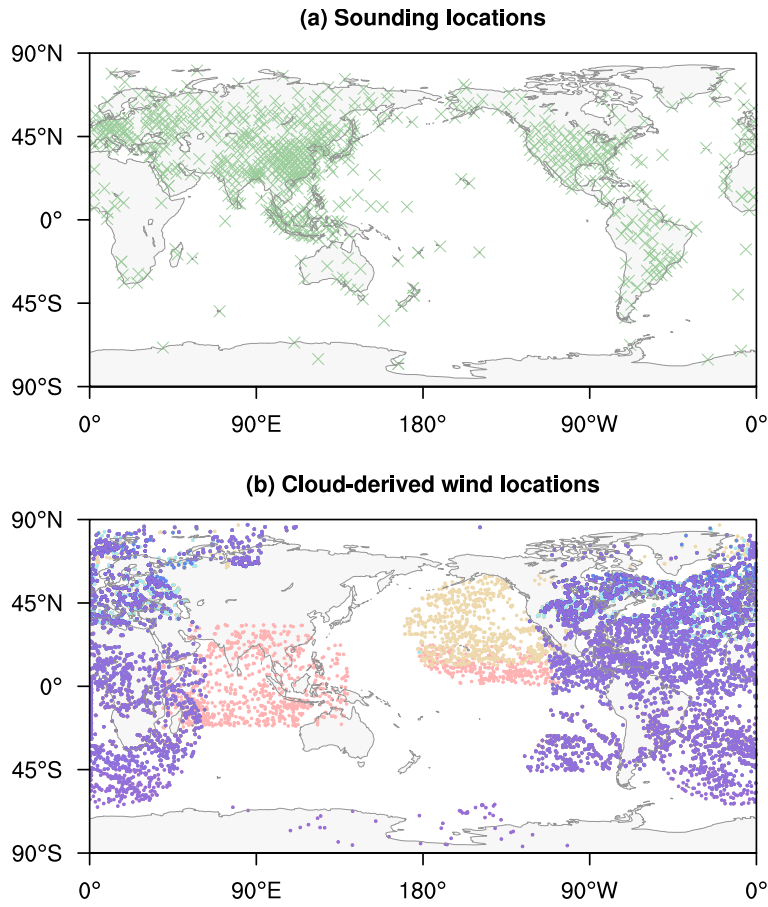
Figure 3. Locations of (a) sounding and (b) cloud-derived wind observations covered the period from 0900 UTC 13 September 2016 to 1500 UTC 13 September 2016. Different colored dots in (b) indicate different sampling times.
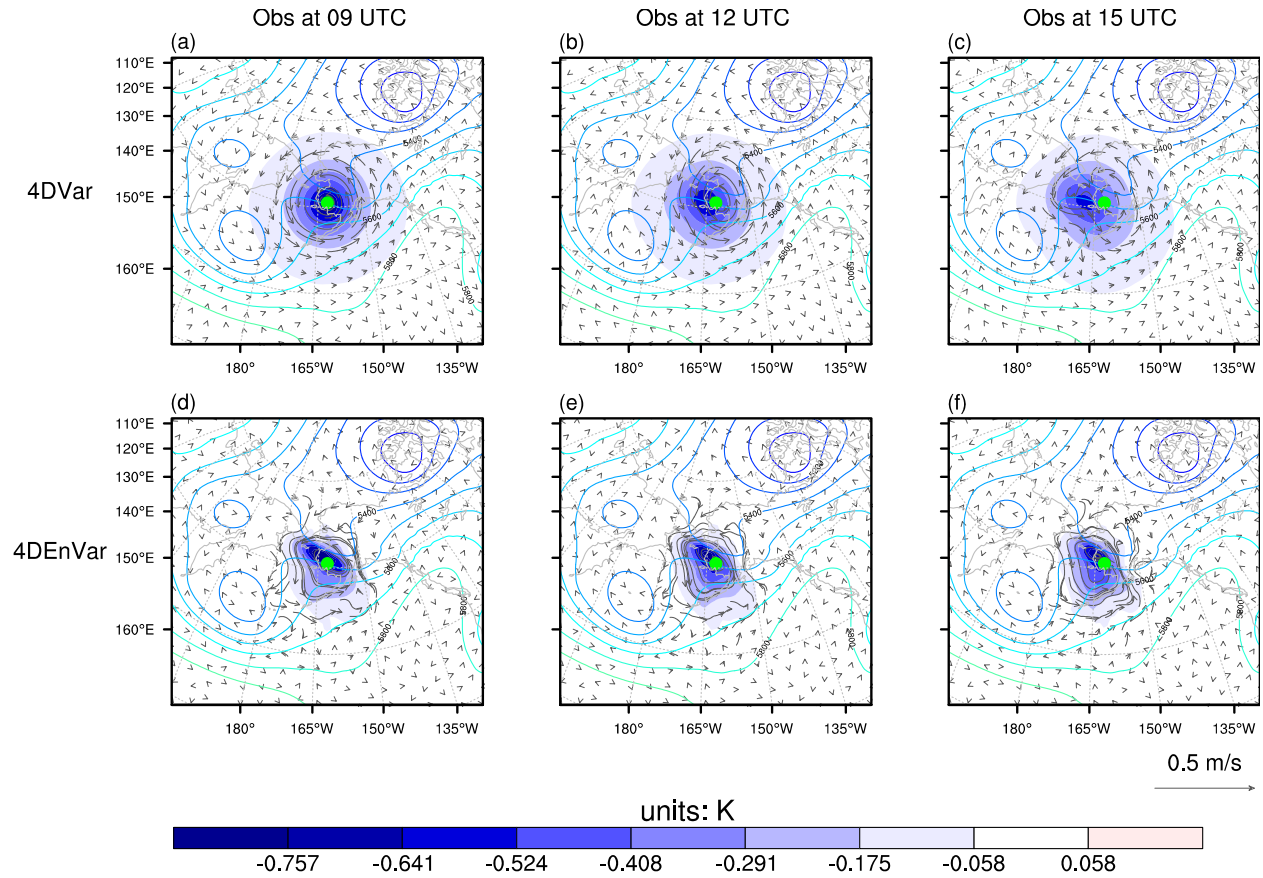
Figure 4. The temperature (shading; units: K) and vector wind (vector; units: m/s) analysis increments from assimilating the single-point temperature observations valid at the (left) beginning, (middle) middle and (right) end of the assimilation window for (top) 4DVar and (bottom) 4DEnVar on the model level closest to the single temperature observation assimilated, which locates at 500hPa (marked with a green dot). The solid contour is the 500hPa background field geopotential height (units: gpm) valid at the beginning of the assimilation window, when the analysis time is taken.

951
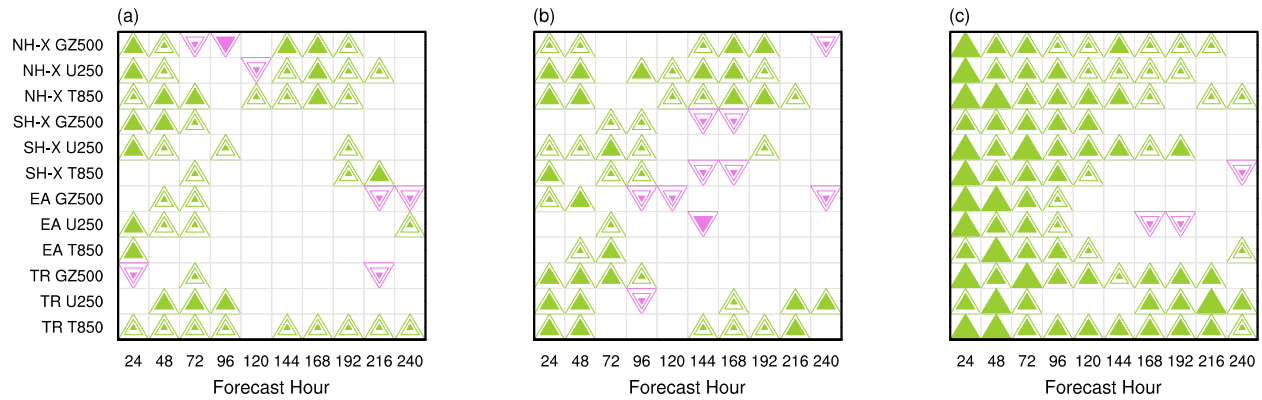
Figure 5. The scorecard of the ARMSE error mean calculated for the forecast initialized by the ensemble mean analysis from the 4DEnVar system adopting inflation coefficients of $(0.2, 0.9)$ against the forecasts from the 4DEnVar system adopting inflation coefficients of (a) $(0.1, 1.0)$, (b) $(0.3, 0.8)$ and (c) $(0.5, 0.6)$ with identical settings, respectively. If the former forecast has a significantly lower (higher) ARMSE error than the latter, then a green upward-pointing (red downward-pointing) triangle is plotted. The corresponding color outline is the three sizes that each symbol can be plotted, and the sizes from large to small corresponds to error mean differences greater than 3 times, between 1 times and 3 times, and between 0.5 times and 1 times the t value of the 95% confidence level, i.e., fairly significant, significant, and insignificant. The graph is not shown when the error mean differences are less than 0.5 times the t value of the 95% confidence level, indicating equivalent.

963

964
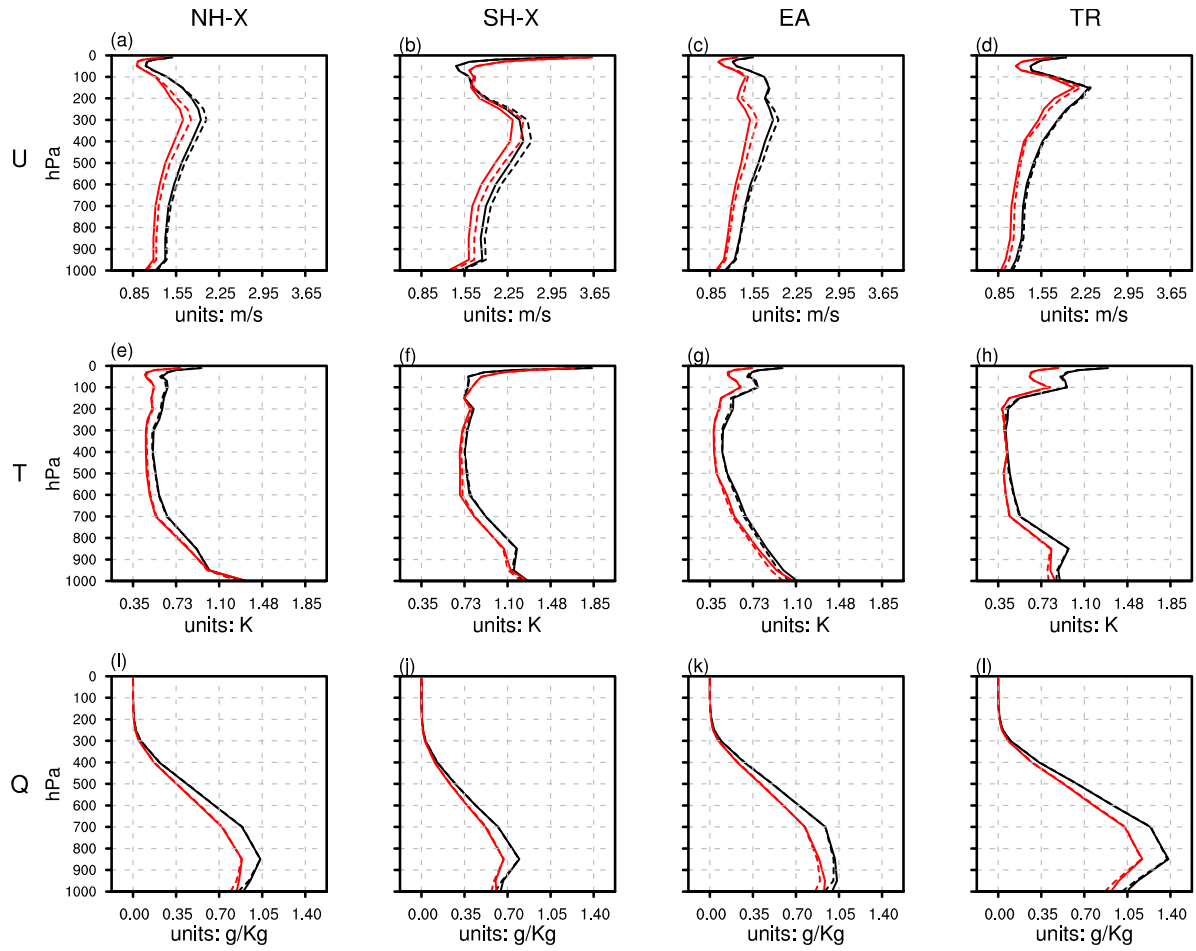
Figure 6. Vertical profiles of the ARMSE (verified relative to the "truth" state) of the background (dashed line) and analysis (solid line) fields of the zonal wind (top; units: m/s), temperature (middle; units: K) and specific humidity (bottom; units: g/Kg) in the Northern Extratropics (20°N~90°N, 180°W~180°E; left), Southern Extratropics (20°S~90°S, 180°W~180°E; middle left), East Asian (15°N~65°N, 70°E~145°E; middle right), and Tropics (20°S~20°N, 180°W~180°E; right). The black and red lines show the 4DVar and 4DEnVar results, respectively.

971
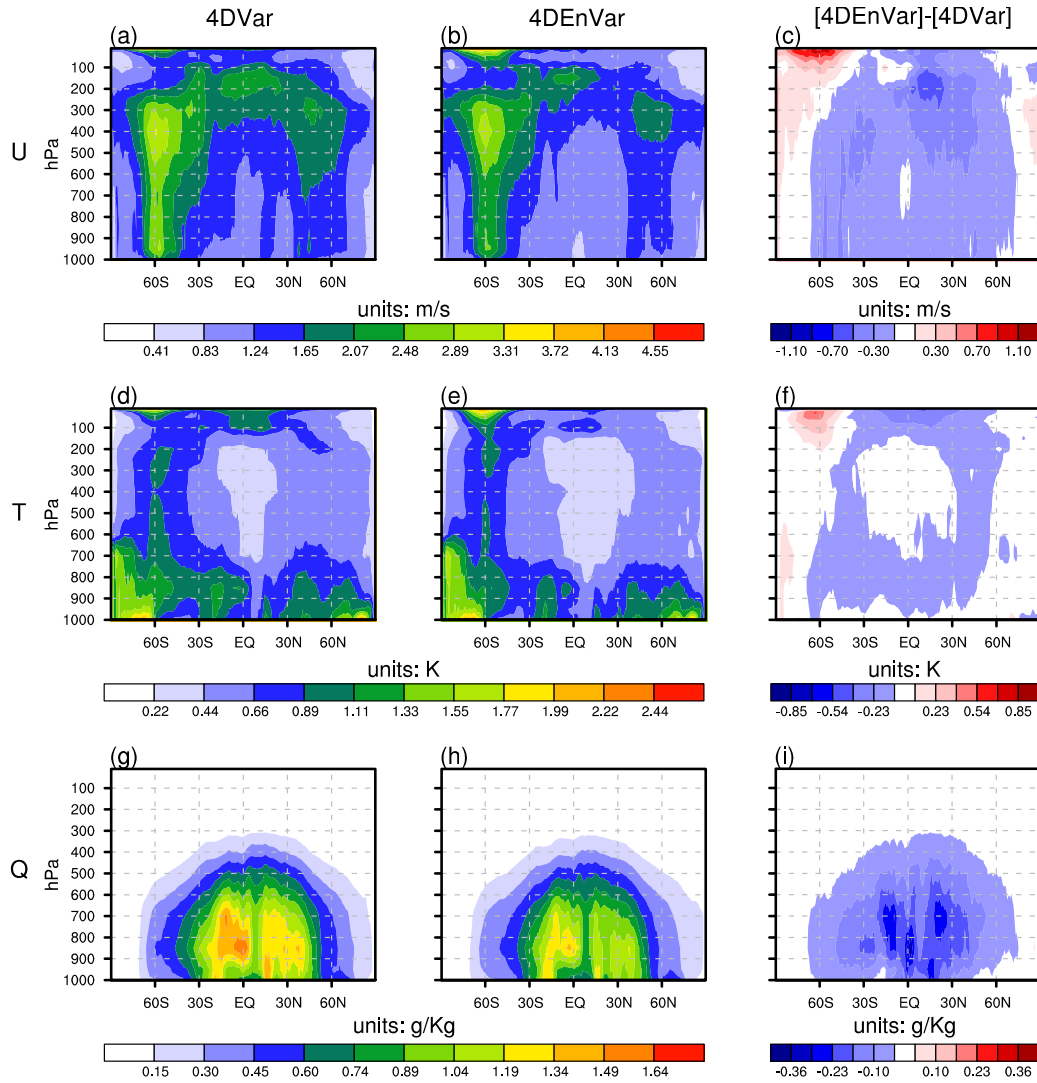
Figure 7. The pressure versus latitude plots of the ARMSEs (verified relative to the "truth" state) of the zonal wind (top; units: m/s), temperature (middle; units: K) and specific humidity (bottom; units: g/Kg) analyses of 4DVar (left), 4DEnVar (middle) and the ARMSE differences between 4DEnVar and 4DVar (right), respectively.

976
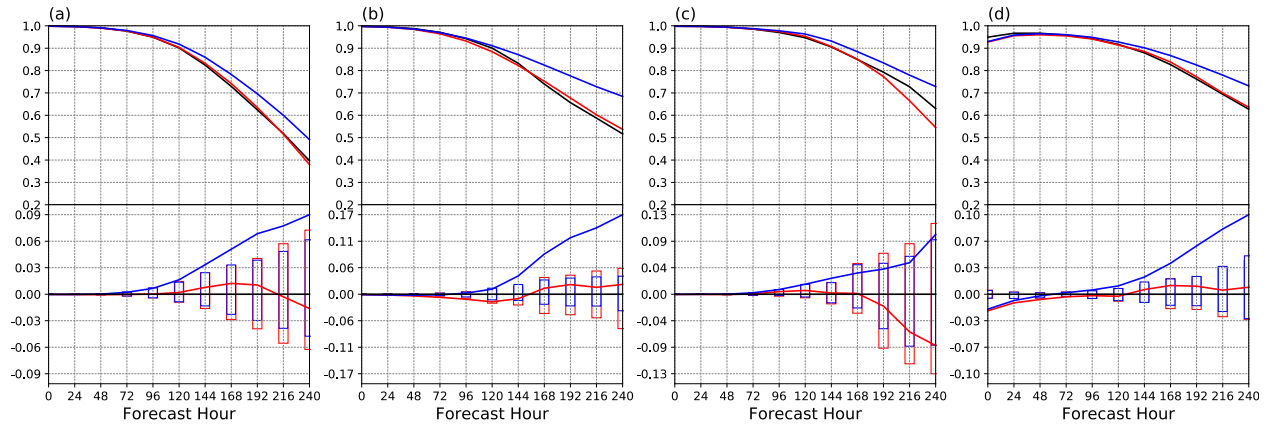
Figure 8. The anomaly correlation coefficients (ACCs) of the 4DVar-based (black line), 4DEnVar-based deterministic (red line) and the 4DEnVar-based ensemble mean (blue line) forecasts of the 500hPa geopotential height against the "truth" state in the (a) Northern Extratropics (20°N~90°N; 180°W~180°E), (b) Southern Extratropics (20°S~90°S; 180°W~180°E), (c) East Asia (15°N~65°N, 70°E~145°E),   and (d) Tropics (20°S~20°N, 180°W~180°E). The corresponding ACC differences between the 4DEnVar-based deterministic forecast and the 4DVar-based forecast (red line), between the 4DEnVar-based ensemble mean forecast and the 4DVar-based forecast (blue line), and the 95% confidence thresholds are also plotted in the bottom.
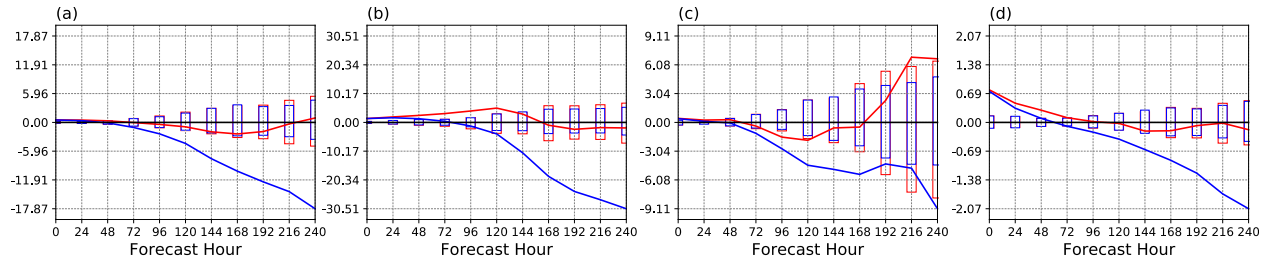
Figure 9. The ARMSE differences between the 4DEnVar-based deterministic forecast and the 4DVar-based forecast (red line) , between the 4DEnVar-based ensemble mean forecast and the 4DVar-based forecast (blue line) of the 500hPa geopotential height against the "truth" state in the (a) Northern Extratropics (20°N~90°N; 180°W~180°E), (b) Southern Extratropics (20°S~90°S; 180°W~180°E), (c) East Asia (15°N~65°N, 70°E~145°E), and (d) Tropics (20°S~20°N, 180°W~180°E). The bar charts show the 95% confidence thresholds.

992
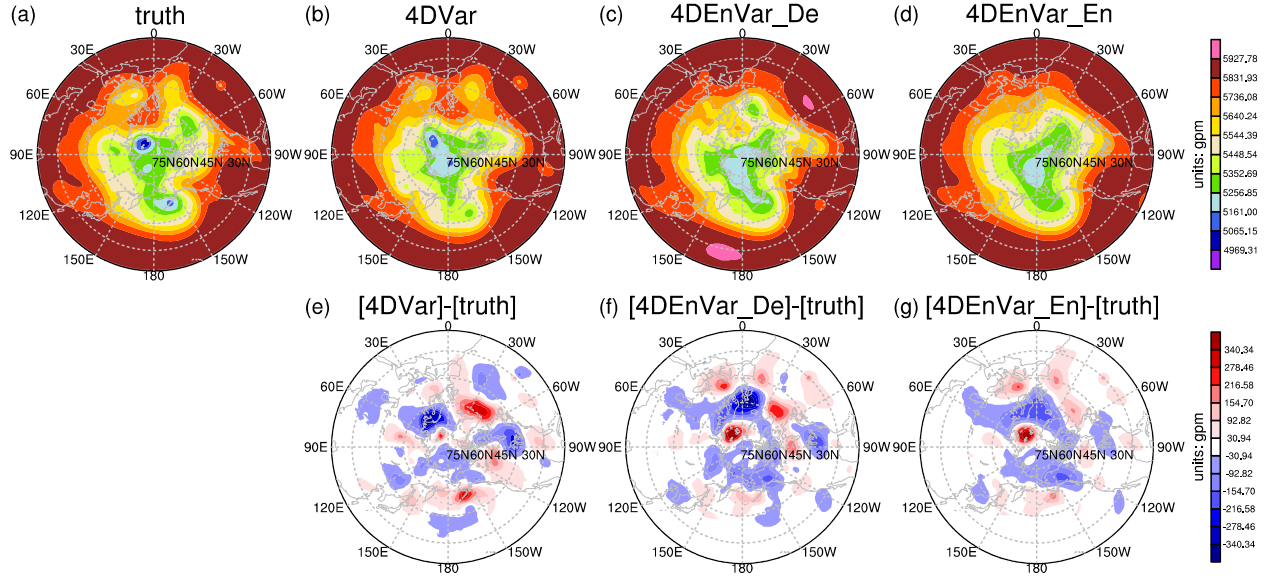
Figure 10. The horizontal distributions of the 240-h forecast of the 500hPa geopotential height in the Northern Extratropics (20°N~90°N; 180°W~180°E) for (a) the "truth" state, (b) the 4DVar-based forecast, (c) the 4DEnVar-based deterministic forecast and (d) the 4DEnVar-based ensemble mean forecast. The differences (e) between the 4DVar-based forecast and the "truth" state, (f) between the 4DEnVar-based deterministic forecast and the "truth" state and (g) between the 4DEnVar-based ensemble mean forecast and the "truth" state are also plotted, respectively.

999
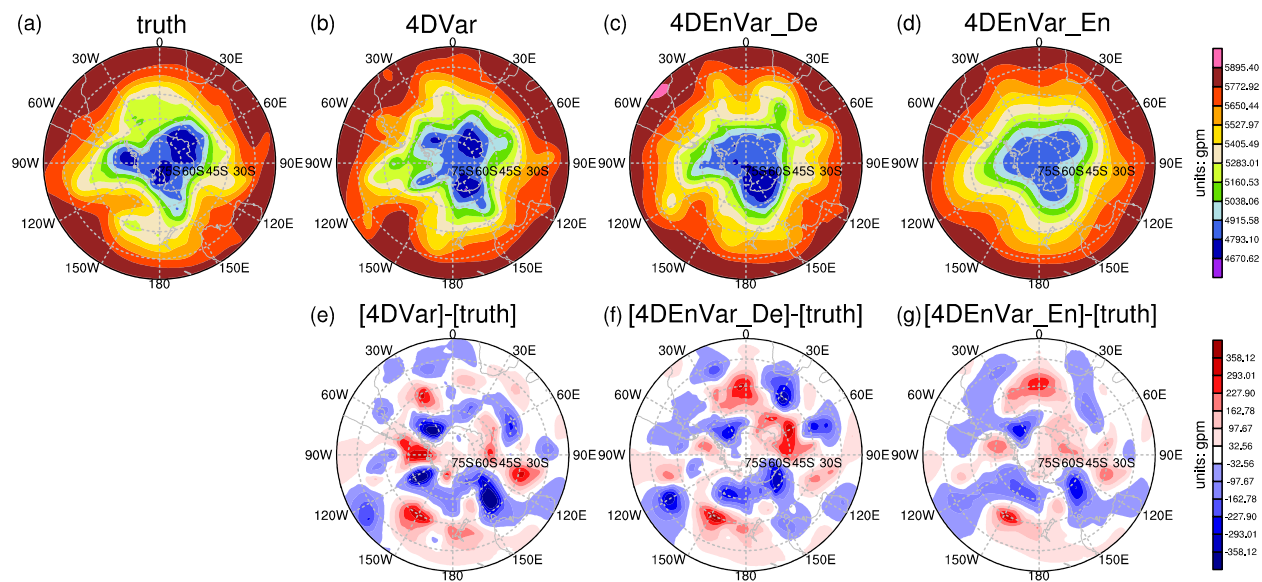
Figure 11. As in Figure 10, but showing the results in the Southern Extratropics (20°S~90°S; 180°W~180°E).

1002
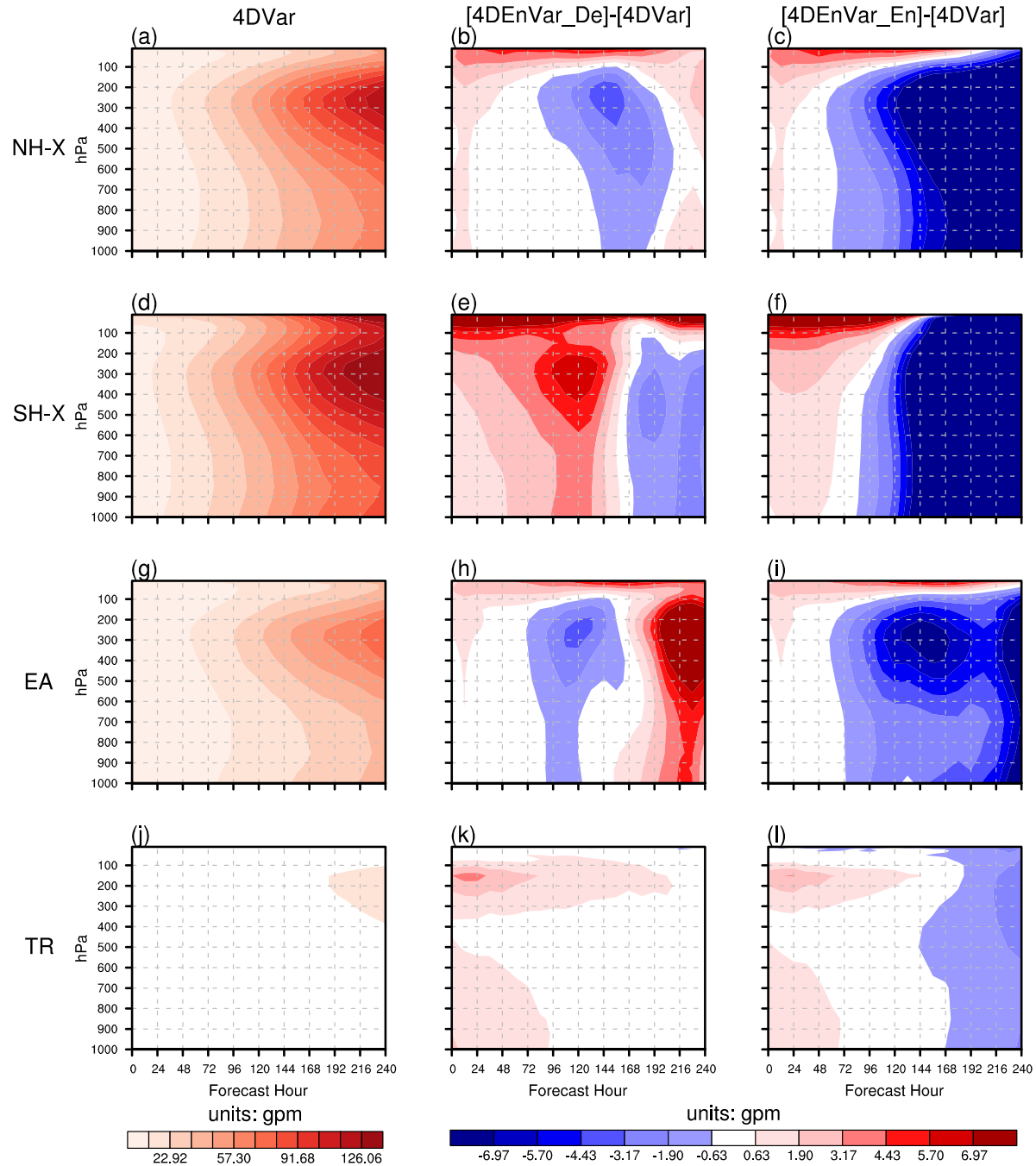
Figure 12. The ARMSEs of the geopotential height forecasts (units: gpm) initiated from the 1200 UTC analyses of the 4DVar experiment as a function of lead time (left) in the (a) Northern Extratropics (20°N~90°N; 180°W~180°E), (d) Southern Extratropics (20°S~90°S; 180°W~180°E), (g) East Asia (15°N~65°N, 70°E~145°E), and (j) Tropics (20°S~20°N, 180°W~180°E). The differences of ARMSE between the 4DEnVar-based deterministic forecast and the 4DVar-based forecast, and between the 4DEnVar-based ensemble mean forecast and the 4DVar-based forecast are plotted in (middle) and (right), respectively.
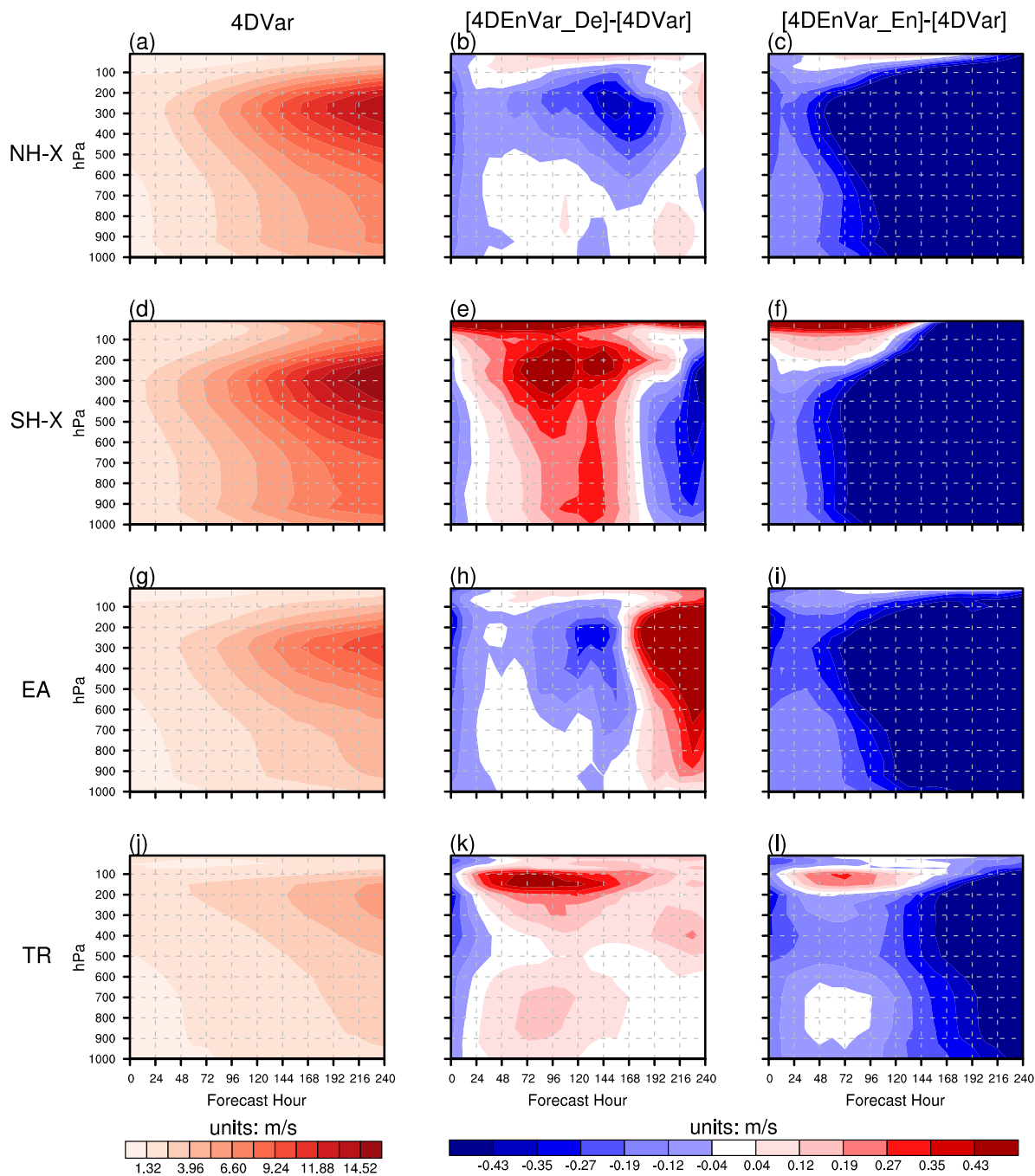
1010

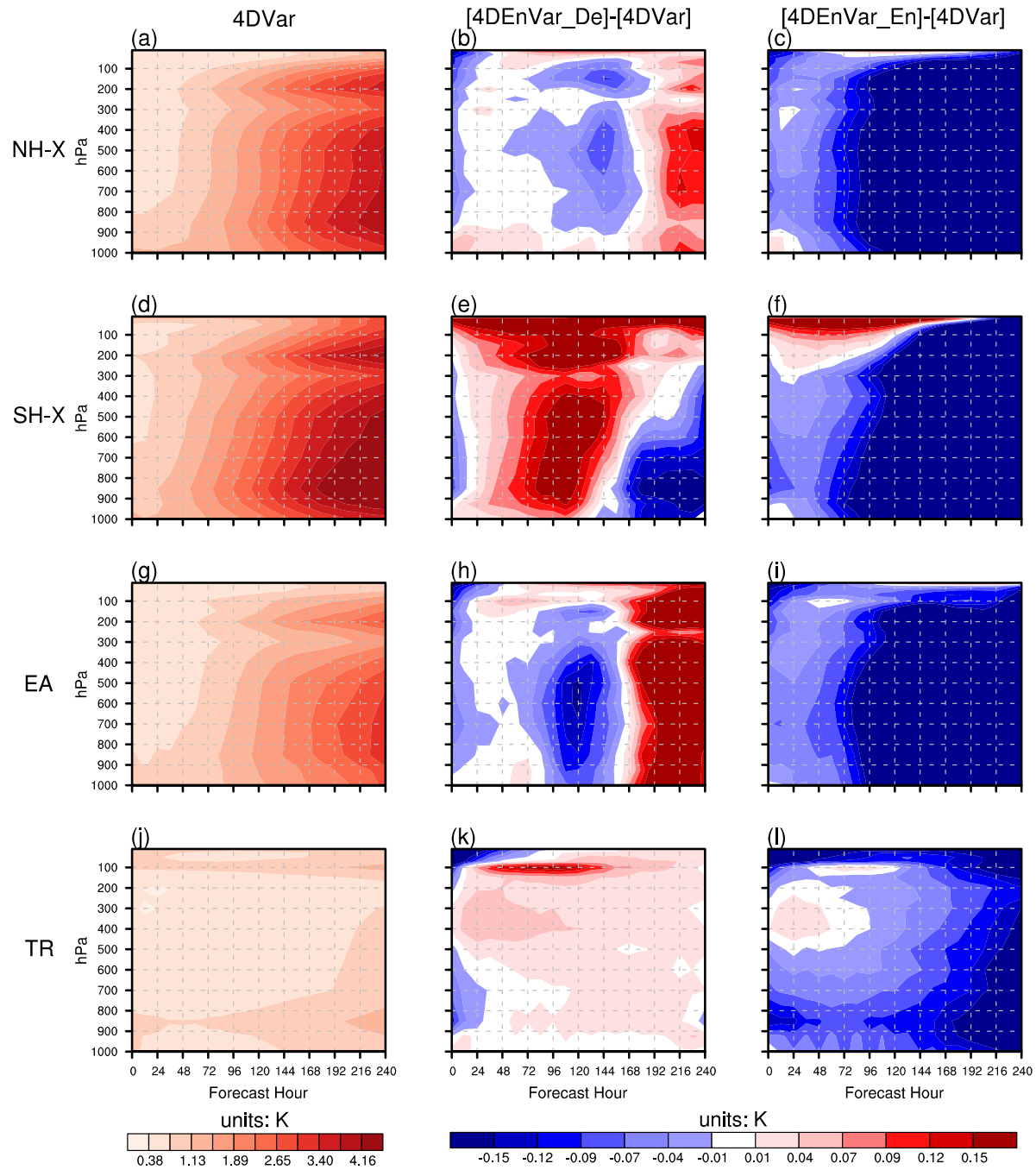1011 **Figure 13**. As in Figure 12, but showing the results of the zonal wind forecasts.

Figure 14. As in Figure 12, but showing the results of the temperature forecasts.
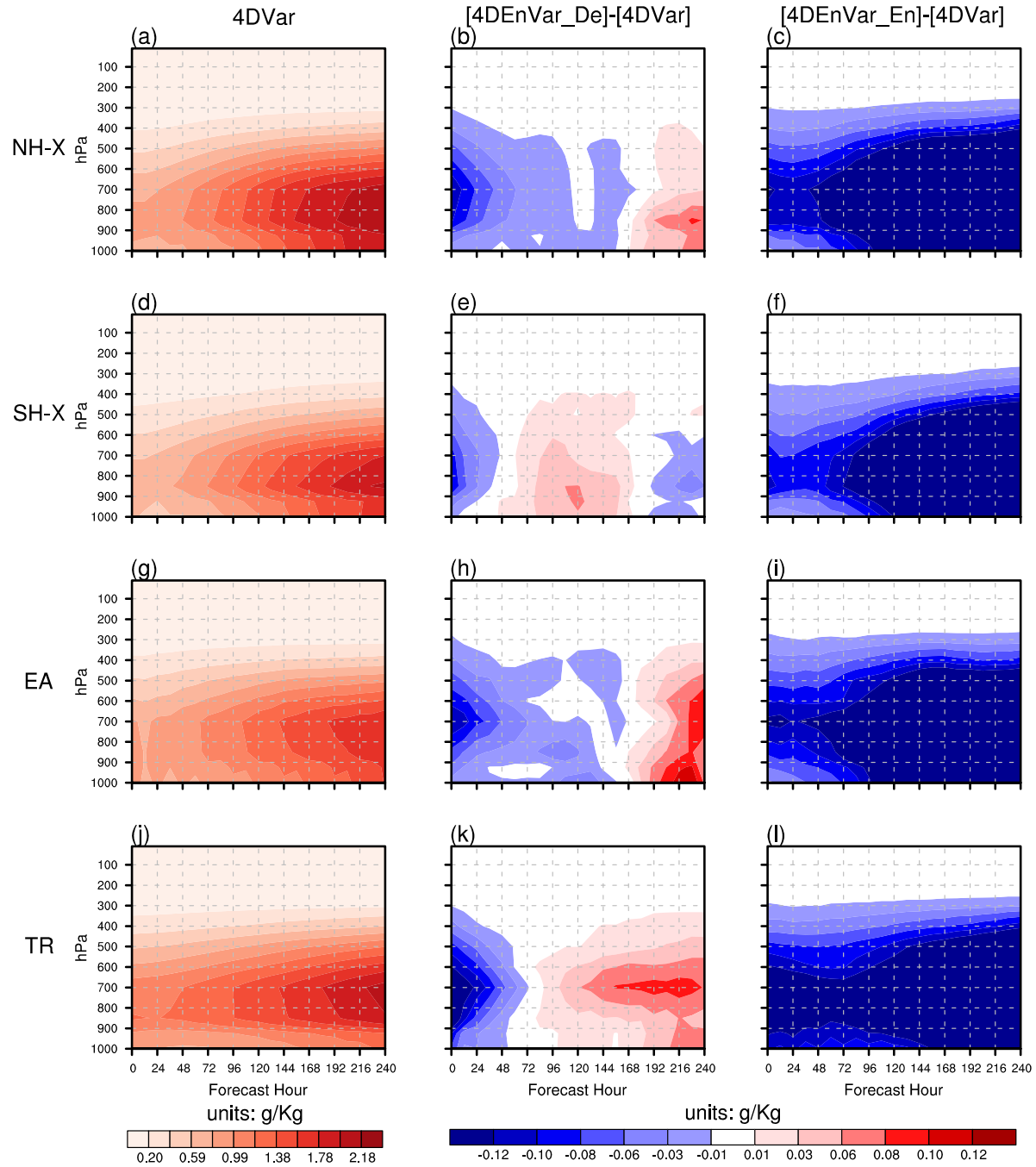
Figure 15. As in Figure 12, but showing the results of the specific humidity forecasts.